Nečas Center for Mathematical Modeling

Algebraic and discretization error estimation by equilibrated fluxes for discontinuous Galerkin methods on nonmatching grids

V. Dolejší, I. Šebestová and M. Vohralík

Preprint no. 2013-022

http://ncmm.karlin.mff.cuni.cz/

Algebraic and discretization error estimation by equilibrated fluxes for discontinuous Galerkin methods on nonmatching grids*

Vít Dolejší† Ivana Šebestová† Martin Vohralík§

August 12, 2013

Abstract

We derive a posteriori error estimates for the discontinuous Galerkin method applied to the Poisson equation. We allow for a variable polynomial degree and simplicial meshes with hanging nodes and propose an approach allowing for simple (nonconforming) flux reconstructions in such a setting. We take into account the algebraic error stemming from the inexact solution of the associated linear systems and propose local stopping criteria for iterative algebraic solvers. An algebraic error flux reconstruction is introduced in this respect. Guaranteed reliability and local efficiency are proven. We next propose an adaptive strategy combining both adaptive mesh refinement and adaptive stopping criteria. At last, we detail a form of the estimates where that factual construction of the reconstructions is not required, which simplifies greatly their evaluation. Numerical experiments illustrate a tight control of the overall error, good prediction of the distribution of both the discretization and algebraic error components, and efficiency of the adaptive strategy.

Key words: linear diffusion problems, discontinuous Galerkin method, a posteriori estimate, flux reconstruction, distribution of the error, error components, stopping criteria, adaptivity, hanging nodes, simple evaluation

Contents

*This work was supported by the ERC-CZ project MORE "MOdelling REvisited + MOdel REduction" LL1202. The research of V. Dolejší was supported by the Grant No. 13-00522S of the Czech Science Foundation. The research of I. Šebestová was supported by the project MathMAC - University center for mathematical modeling, applied analysis and computational mathematics of the Charles University in Prague.

†Department of Numerical Mathematics, Charles University in Prague, Sokolovská 83, 186 75 Praha 8, Czech Republic (dolejsi@karlin.mff.cuni.cz, ivana.sebestova@karlin.mff.cuni.cz).

§INRIA Paris-Rocquencourt, B.P. 105, 78153 Le Chesnay, France (martin.vohralik@inria.fr).

1 Introduction

We consider the second-order pure diffusion problem

$$-\Delta u = f \quad \text{in } \Omega, \tag{1.1a}$$
$$u = 0 \quad \text{on } \partial\Omega, \tag{1.1b}$$

where $\Omega \subset \mathbb{R}^d$, $d = 2$ or 3, is a polygonal (polyhedral) domain and f a source term. The homogeneous Dirichlet boundary condition (1.1b) is only considered for the sake of simplicity. Hereafter, u is termed the *potential* and $-\nabla u$ the *flux*. We assume that $f \in L^2(\Omega)$, so that the model problem (1.1) admits a unique weak solution u.

The total error in a computational approximation of (1.1) consists of two parts: the *discretization error*, which arises due to the transition from the infinite-dimensional mathematical model to a finite-dimensional numerical approximation, and the *algebraic error*, which arises due to inaccurate solution of the underlying algebraic systems. Despite a large number of papers dedicated to error estimates, most of them *do not* take into account the algebraic error. Among those that do, let us cite [7, 4, 6, 20, 15, 14]. As pointed out in these references, see also [5] and [19, Chapter 5], knowledge of the algebraic error is of significant importance for an *efficient numerical solution* of partial differential equations. The key idea is that of balancing of the discretization and algebraic errors through *a posteriori error estimates* and *stopping criteria* for iterative algebraic solvers.

Such an idea has already appeared in [7]. A posteriori error estimates involving both discretization and algebraic error in H^1 and L^2 norms have been derived there for the Poisson equation considering a piecewise linear finite element approximation together with a multigrid algebraic solver. A stopping criterion for the solver has been proposed. The approach is based on a strong stability and the orthogonality property. Numerical examples illustrate its reliability and efficiency. In [4], stopping criteria for the conjugate gradient method with respect to the finite element discretization have been studied. The result is based on a lower bound of the energy norm of the algebraic error of the conjugate gradient method. An extension for non-self-adjoint problems has been carried out in [6]. Goal-oriented a posteriori error analysis for a linear elliptic problem focusing on the multigrid method has been carried out in [20]. This concept has been later applied to the linear elliptic eigenvalue problem in [24]. A linear diffusion problem discretized by a finite volume method with a focus on the conjugate gradient solver is a subject of the study in [15]. Recently, a general framework for adaptive numerical solution of nonlinear partial differential equations of diffusion type has been given in [14]. A posteriori error estimates distinguishing the individual error components together with stopping criteria for both iterative linear and nonlinear solvers have been developed therein.

It has been illustrated in [19] that even for simple model problems, the *local distribution* of the discretization and algebraic *errors* can differ significantly. It may happen that the overall discretization error dominates the overall algebraic one, whereas locally, it is just the opposite. Congruently, the stopping criteria proposed in [15, 14] are based on the *local balancing* of the discretization and algebraic errors. This typically leads to *local efficiency* of the estimates even in presence of the algebraic error. Thus, the adaptive computational process can be carried out safely including *adaptive mesh refinement*.

The presence of hanging nodes in the computational mesh is rather seldom allowed in a posteriori error analysis. In the context of the so-called equilibrated fluxes, it has been done by prescription of the local degrees of freedom of the flux for advection–diffusion–reaction problems on nonmatching simplicial meshes in [12]. Pure diffusion problems with non-uniform polynomial degree of the approximate solution are treated in [2, 3]. In [13], almost arbitrary polygonal/polyhedral meshes are considered and the flux is constructed

by solving local Neumann problems. All these approaches require existence of a matching submesh of the given nonmatching mesh to obtain a $\mathbf{H}(\mathrm{div},\Omega)$-conforming flux reconstruction, whereas an approach not requiring a matching submesh is presented in [22, Section 6], following an idea from [29].

In this paper, we aim at extending existing equilibrated flux a posteriori error estimates for discontinuous Galerkin methods (DGMs) by including the algebraic error, permitting hanging nodes (without the necessity to construct any submesh), and allowing the polynomial degree of the approximate solution to vary locally. We also focus on facilitating the evaluation of the estimators; at least for low-order approximations, the resulting formulas featuring different flux reconstructions can be rewritten in a simple form where in particular the factual construction of flux reconstructions is not required. Our error estimates are derived in the broken energy norm with the aid of a flux reconstruction that is constructed in broken Raviart–Thomas–Nédélec (RTN) space; unlike the existing approaches in the literature, our proposed approach operates on the original nonmatching mesh only. Therefore, our flux reconstructions generally fail to belong to $\mathbf{H}(\mathrm{div},\Omega)$ and flux-nonconformity estimators appear.

The reconstructed flux consists of the discretization and algebraic components. Following the approach introduced in [15, 14], the algebraic component is constructed directly from the discretization flux reconstruction by performing some additional steps of the iterative algebraic solver. Such a construction is not computationally expensive, as the forward iterations are used at the next step of the algebraic solver, but it does not lead to the exact equilibration property of the flux reconstruction. A remainder term appears which is treated as in [14].

This paper is organized as follows. We introduce the continuous and discrete settings in Section 2. A guaranteed a posteriori error estimate taking into account nonmatching meshes, varying polynomial degrees, and the algebraic error is derived in Section 3. Local adaptive stopping criteria are devised in Section 4. Section 5 then proves local efficiency even in the considered complex setting. The discussion of simple practical implementation of the derived a posteriori estimates is presented in Section 6. Finally, Section 7 with numerical experiments demonstrating the tight prediction of the distribution of both the discretization and algebraic errors even on meshes with hanging nodes concludes the paper.

2 Continuous and discrete problems

We set up here our notation and introduce the continuous and discrete problems.

2.1 Continuous problem

We use standard notation for the Lebesgue and Sobolev spaces. Specifically, for a given domain $M \subset \mathbb{R}^d$, $L^2(M)$ denotes the space of square-integrable functions and $H^1_0(M)$ the space of functions having square-integrable weak derivatives up to the first order and traces vanishing on the boundary. Further, $(\cdot,\cdot)_M$ denotes the inner product in $L^2(M)$ or $[L^2(M)]^d$, $\|\cdot\|_M$ denotes the induced norm, and $(\cdot,\cdot)_{\partial M}$ denotes $(d-1)$-dimensional $L^2(\partial M)$ inner product on ∂M. We will omit subscript M in case $M=\Omega$. By $\mathbf{H}(\mathrm{div},M) := \{\mathbf{v}\in[L^2(M)]^d; \nabla\cdot\mathbf{v}\in L^2(M)\}$ we denote the space with square-integrable weak divergences, see, e.g., [8] or [23]. Let us introduce the weak formulation of the problem (1.1): Find $u\in H^1_0(\Omega)$ such that

$$(\nabla u,\nabla v) = (f,v) \quad \forall v\in H^1_0(\Omega). \tag{2.1}$$

2.2 Meshes with hanging nodes

We consider a family $\mathcal{T}_h$ ($h>0$) of partitions of the closure of Ω into a finite number of closed triangles in 2D and tetrahedra in 3D. We suppose that the simplices have mutually disjoint interiors but we *admit* the presence of the so-called *hanging nodes*. This means that the condition that any face of any element K in the partition is either a subset of the boundary $\partial\Omega$ or a face of another element K' may be violated.

We assume that any mesh $\mathcal{T}_h$ was formed from some initial simplicial mesh without hanging nodes by subdividing some of its elements (repeatedly) into $(d+1)+(d-1)^2$ congruent simplices. Thus, for each $K\in\mathcal{T}_h$ with a face possessing a hanging node, there exists a simplex, called macro-simplex, sharing this entire face. Note that macro-elements are not included in the mesh $\mathcal{T}_h$. Fig. 1, left gives an illustration of an admissible mesh and an example of the macro-element.

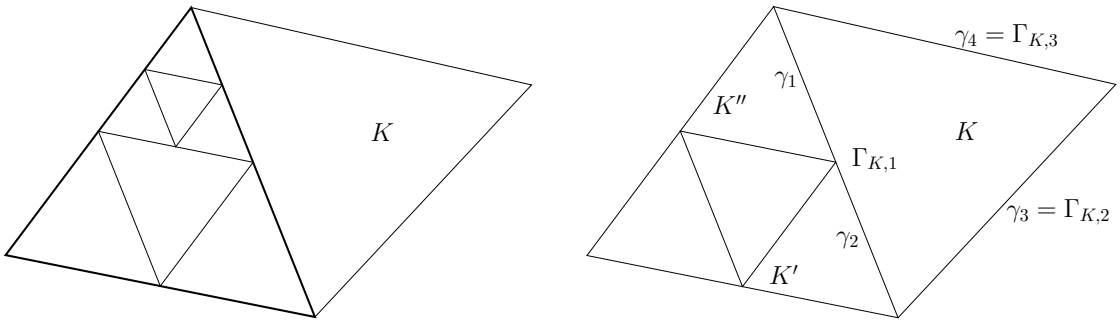

Figure 1: Example of K having a face with hanging nodes and the macro-element (bold) sharing this face (left). Notation of the symbols Γ and γ: entire faces $\Gamma_{K,i},\ i = 1, 2, 3$, of the element K with a hanging node and the sub-faces $\gamma_j,\ j = 1, \ldots, 4$; obviously $\Gamma_{K,1} = \gamma_1 \cup \gamma_2$ (right).

Due to a possible presence of hanging nodes, we have to distinguish two types of faces. First, each simplex $K \in \mathcal{T}_h$ has $d+1$ faces Γ defining its boundary ∂K. Second, if a face Γ of some $K \in \mathcal{T}_h$ contains (a) hanging node(s) then Γ can be split into several sub-faces $\gamma \subset \Gamma$ where $\gamma = \partial K \cap \partial K'$ for some $K' \in \mathcal{T}_h$. Hence, the symbol Γ denotes an entire face of some $K \in \mathcal{T}_h$ whereas the symbol γ its part which is a common boundary between two neighboring elements. If $\Gamma \subset \partial K$ does not contain a hanging node then there exists $\gamma \subset \partial K$ such that $\gamma = \Gamma$, see Fig. 1, right.

By $\mathcal{E}_K$ we denote the set of all faces $\Gamma \subset \partial K$, by $\mathcal{E}_K^{\mathrm{HG}}$ those of them that contain at least one hanging node, and by $\mathcal{E}_K^{\mathrm{I}}$ the faces of $\mathcal{E}_K$ lying in the interior of Ω. Additionally, we set

$$\mathcal{E}_K^{\mathrm{HG,N}} := \{\Gamma \in \mathcal{E}_K^{\mathrm{I}} \setminus \mathcal{E}_K^{\mathrm{HG}}, \Gamma \nsubseteq \Gamma' \in \mathcal{E}_{K'}^{\mathrm{HG}}, K' \in \mathcal{T}_h\}, \tag{2.2}$$

which denotes the set of all faces of $K \in \mathcal{T}_h$ which *are not* a part of a face with a hanging node of the neighboring element, see Figure 2. Obviously, if $\Gamma \in \mathcal{E}_K^{\mathrm{HG,N}}$ then there exists $\gamma = \partial K \cap \partial K'$ for some $K' \in \mathcal{T}_h$ such that $\gamma = \Gamma$.

Furthermore, we define the sets of interior and boundary faces γ (edges for $d = 2$) of $\mathcal{T}_h$ as follows:

$$\mathcal{F}_h^{\mathrm{I}} = \{\gamma;\ \gamma = \partial K \cap \partial K', |\gamma| > 0, K, K' \in \mathcal{T}_h\}, \tag{2.3a}$$

$$\mathcal{F}_h^{\mathrm{B}} = \{\gamma;\ \gamma \text{ is a face of } K, \gamma \subset \partial K \cap \partial\Omega, K \in \mathcal{T}_h\}, \tag{2.3b}$$

where $|\gamma|$ stands for the $(d-1)$-dimensional Lebesgue measure of γ, and set $\mathcal{F}_h := \mathcal{F}_h^{\mathrm{I}} \cup \mathcal{F}_h^{\mathrm{B}}$. For each $\gamma \in \mathcal{F}_h^{\mathrm{I}}$, we use the notation K_γ^{L} and K_γ^{R} for the two elements, called neighbors hereafter, such that $\gamma = \partial K_\gamma^{\mathrm{L}} \cap \partial K_\gamma^{\mathrm{R}}$. Hence, for the example pictured in Fig. 1, right, we have $K_{\gamma_1}^{\mathrm{L}} = K''$, $K_{\gamma_1}^{\mathrm{R}} = K$, $K_{\gamma_2}^{\mathrm{L}} = K'$ and $K_{\gamma_2}^{\mathrm{R}} = K$. We define a unit normal vector $\mathbf{n}_\gamma$ to each $\gamma \in \mathcal{F}_h^{\mathrm{I}}$ so that it points out of K_γ^{L}. We assume that $\mathbf{n}_\gamma$, $\gamma \in \mathcal{F}_h^{\mathrm{B}}$, coincides with the unit outward normal to $\partial\Omega$. Note that a face of an element that is divided into several parts due to the presence of (a) hanging node(s) has, in fact, several parallel normal vectors (possibly with different orientation). Let $h_\gamma := \mathrm{diam}(\gamma)$ for $\gamma \in \mathcal{F}_h$, $h_K := \mathrm{diam}(K)$ for $K \in \mathcal{T}_h$, let $|K|$ denote the Lebesgue measure of an element K, ∂K the boundary of K, and $|\partial K|$ the $(d-1)$-dimensional Lebesgue measure of ∂K.

The previous notations give the identity

$$\bigcup_{K\in\mathcal{T}_h} \partial K = \bigcup_{K\in\mathcal{T}_h} \Big\{ \Big(\bigcup_{\Gamma\in\mathcal{E}_K^{\mathrm{HG}}} \Gamma \Big) \bigcup \Big(\bigcup_{\Gamma\in\mathcal{E}_K^{\mathrm{HG,N}}} \Gamma \Big) \bigcup \Big(\bigcup_{\gamma\in\mathcal{E}_K\cap\mathcal{F}_h^{\mathrm{B}}} \gamma \Big) \Big\}. \tag{2.4}$$

Obviously, all faces having a hanging node belong to the first union, all interior faces without hanging nodes and not being a part of a face with a hanging node of the neighboring element appear in the second union two times, and all boundary faces appear in the third union. Notice that boundary faces do not possess hanging nodes, i.e. $\mathcal{E}_K^{\mathrm{HG}} \cap \mathcal{F}_h^{\mathrm{B}} = \emptyset$, $K \in \mathcal{T}_h$ and $\gamma = \Gamma$ for $\gamma \in \mathcal{F}_h^{\mathrm{B}}$.

We let $\mathcal{T}_K$ stand for the set of the element K itself and its neighbors, which includes all elements of $\mathcal{T}_h$ that are contained in the macro-elements sharing a complete face with the element K in case that K

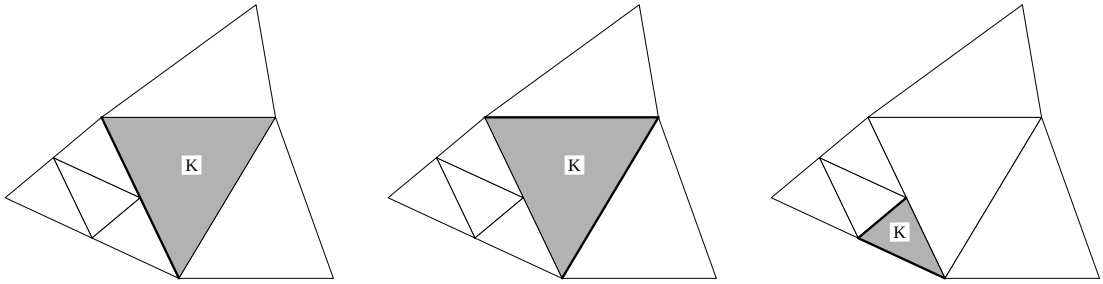

Figure 2: An example of the set of faces (bold lines) $\mathcal{E}_K^{\mathrm{HG}}$ of an element with a hanging node (left), the set of faces $\mathcal{E}_K^{\mathrm{HG,N}}$ of an element with a hanging node (center) and the set of faces $\mathcal{E}_K^{\mathrm{HG,N}}$ of an element whose vertex gives rise to a hanging node of the neighboring element (right).

possesses (a) hanging node(s). Further, $\mathcal{F}_K$ denotes all the faces in this patch and $\widetilde{\mathcal{F}}_K$ stands for the set of faces that share at least a vertex with K.

We assume that the following conditions are satisfied:

$$\text{shape regularity:} \quad \exists C_{\mathrm{s}} > 0;\ \frac{h_K}{\rho_K} \le C_{\mathrm{s}} \quad \forall K \in \mathcal{T}_h, \tag{2.5a}$$

$$\text{local quasi-uniformity:} \quad \exists C_H > 0;\ h_K \le C_H h_{K'} \quad \forall K, K' \in \mathcal{T}_h \ \text{ neighbors}, \tag{2.5b}$$

where ρ_K denotes the diameter of the largest d-dimensional ball inscribed into K.

2.3 Broken spaces

We define the so-called broken Sobolev space over the mesh $\mathcal{T}_h$,

$$H^s(\Omega, \mathcal{T}_h) = \{v \in L^2(\Omega); v|_K \in H^s(K) \quad \forall K \in \mathcal{T}_h\},\ s \ge 1.$$

We equip it with the norm $\|v\|^2_{H^s(\Omega,\mathcal{T}_h)} := \sum_{K\in\mathcal{T}_h} \|v\|^2_{H^s(K)}$. For $v \in H^1(\Omega, \mathcal{T}_h)$, we define the broken gradient $\nabla_h v$ of v by $(\nabla_h v)|_K := \nabla(v|_K)$ for all $K \in \mathcal{T}_h$ and use the following notation: v_γ^{L} stands for the trace of $v|_{K_\gamma^{\mathrm{L}}}$ on γ, v_γ^{R} is the trace of $v|_{K_\gamma^{\mathrm{R}}}$ on γ, $\langle v\rangle_\gamma := \frac{1}{2}(v_\gamma^{\mathrm{L}} + v_\gamma^{\mathrm{R}})$, $[v]_\gamma := v_\gamma^{\mathrm{L}} - v_\gamma^{\mathrm{R}}$, $\gamma \in \mathcal{F}_h^{\mathrm{I}}$. Further, for $\gamma \in \mathcal{F}_h^{\mathrm{B}}$, we define v_γ^{L} as the trace of $v|_{K_\gamma^{\mathrm{L}}}$ on γ, and $\langle v\rangle_\gamma := [v]_\gamma := v_\gamma^{\mathrm{L}}$. If $[\cdot]_\gamma$ or $\langle\cdot\rangle_\gamma$ appear in an integral of the form $\int_\gamma \dots \mathrm{d}S$, we will omit the subscript γ and write, respectively, $[\cdot]$ and $\langle\cdot\rangle$ instead.

To each $K \in \mathcal{T}_h$ we assign an integer $p_K \ge 1$ and set $\boldsymbol{p} := \{p_K\}_{K\in\mathcal{T}_h}$. Then, we define the space of discontinuous piecewise polynomials

$$S_h^{\boldsymbol{p}} = \{v \in L^2(\Omega); v|_K \in \mathbb{P}^{p_K}(K) \quad \forall K \in \mathcal{T}_h\},$$

where $\mathbb{P}^{p_K}(K)$ is the space of polynomials on K of degree at most p_K. We let $N := \dim(S_h^{\boldsymbol{p}})$ and $N_K := \dim(\mathbb{P}^{p_K}(K))$.

2.4 The discontinuous Galerkin method

We discretize the problem (1.1) with the aid of the *interior penalty discontinuous Galerkin method*, see, e.g., [10] and the references therein. Hence, for $u_h, v_h \in S_h^{\boldsymbol{p}}$, we define the forms

$$\begin{aligned} a(u_h, v_h) := &\sum_{K\in\mathcal{T}_h} (\nabla u_h, \nabla v_h)_K - \sum_{\gamma\in\mathcal{F}_h} (\langle\nabla u_h\rangle\cdot\mathbf{n}_\gamma, [v_h])_\gamma \\ &- \theta \sum_{\gamma\in\mathcal{F}_h} (\langle\nabla v_h\rangle\cdot\mathbf{n}_\gamma, [u_h])_\gamma + \sum_{\gamma\in\mathcal{F}_h} (\alpha_\gamma h_\gamma^{-1}[u_h], [v_h])_\gamma, \end{aligned} \tag{2.6a}$$

$$\ell(v_h) := (f, v_h), \tag{2.6b}$$

where $\alpha_\gamma > 0$, $\gamma \in \mathcal{F}_h$, are (sufficiently large) penalty parameters, and the parameter $\theta \in \{1, -1, 0\}$ corresponds to the symmetric, nonsymmetric, and incomplete variants of the interior penalty DGM, respectively. The discontinuous Galerkin method for problem (1.1) then reads:

$$\text{Find } u_h \in S_h^{\boldsymbol{p}} \text{ such that } a(u_h, v_h) = \ell(v_h) \quad \forall v_h \in S_h^{\boldsymbol{p}}. \tag{2.7}$$

2.5 Algebraic solution of the linear systems

Let $\{\varphi_l\}_{l=1\dots N}$ be a basis of the space $S_h^{\boldsymbol{p}}$ such that support of each φ_l, $l = 1, \dots, N$, is just one simplex $K \in \mathcal{T}_h$. Then, expressing the solution of (2.7) in this basis, $u_h = \sum_{l=1}^{N} U_{h,l}\varphi_l$, (2.7) can be rewritten in the matrix form as follows:

$$\text{Find } U_h \in \mathbb{R}^N \text{ such that } \mathbb{A}U_h = F, \tag{2.8}$$

where $\mathbb{A} = \{\mathbb{A}_{kl}\}_{k,l=1\dots N} := \{a(\varphi_l, \varphi_k)\}_{k,l=1\dots N}$, $U_h := \{U_{h,l}\}_{l=1\dots N}$, and $F = \{F_k\}_{k=1\dots N} := \{\ell(\varphi_k)\}_{k=1\dots N}$.

Using an iterative algebraic method, the linear algebraic system (2.8) is *not solved exactly*; at i-th iteration step, we have

$$\mathbb{A}U_h^i = F - R^i, \tag{2.9}$$

where R^i is the algebraic residual vector associated with the available approximation U_h^i. In other words, the solution that we have at our disposal at step i solves the algebraic system with a perturbed right-hand side.

Let us define the residual function $r_h^i \in S_h^{\boldsymbol{p}}$ by $(r_h^i, \varphi_k) = R_k^i$ for $k = 1 \dots N$. Then the system (2.9) represents the following perturbed discontinuous Galerkin problem:

$$\text{Find } u_h^i \in S_h^{\boldsymbol{p}} \quad \text{such that} \quad a(u_h^i, v_h) = \ell(v_h) - (r_h^i, v_h) \quad \forall v_h \in S_h^{\boldsymbol{p}}. \tag{2.10}$$

3 Guaranteed error upper bound

In this section, we derive a posteriori error estimate on the error between the approximation u_h^i available from (2.10) and the unknown weak solution u of (2.1).

3.1 Averaging interpolation operator

We first need to construct a $H_0^1(\Omega)$-conforming piecewise polynomial interpolation of a discontinuous piecewise polynomials on nonmatching meshes. We follow the approach based on averaging from [16], where the construction has been done for uniform polynomial degree over a mesh possibly containing hanging nodes. In [3], an extension for a varying polynomial degree considering a matching submesh has been carried out. Our proposed approach operates on the *original nonmatching mesh only* and extends that of [16].

For $v_h \in S_h^{\boldsymbol{p}}$, we intend to define a function $\mathcal{I}_{\mathrm{Av}}(v_h)$ having a polynomial degree in the interior of each element $K \in \mathcal{T}_h$ equal to maximum of polynomial degrees of v_h in some neighborhood. For elements *without* a face being a part of a face with a hanging node, the maximum is taken over neighboring elements. For elements *with* such a face, the maximum is also taken over elements sharing the face with the hanging node. We set $\mathcal{I}_{\mathrm{Av}}(v_h)$ to be a polynomial of possibly *lower degree* on a face $\Gamma \in \mathcal{E}_K$, $K \in \mathcal{T}_h$, given by the maximum of polynomial degrees of elements sharing this face and in case this face is a part of a face with a hanging node elements sharing the face with the hanging node. Such a construction prevents excessive refinement in the vicinity of elements with a high polynomial degree. Figure 3 gives an example of a mesh with hanging nodes and varying polynomial degree of the approximate solution (left) and the corresponding polynomial degree of the interpolation operator $\mathcal{I}_{\mathrm{Av}}$ together with its degrees of freedom (right).

For $\Gamma \in \mathcal{E}_K^{\mathrm{HG,N}} \cup \mathcal{E}_K^{\mathrm{HG}} \cup \mathcal{F}_h^{\mathrm{B}}$, $K \in \mathcal{T}_h$, we denote $p_\Gamma := \max\{p_{K'}; |\Gamma \cap \partial K'| > 0\}$. For $\Gamma \in \mathcal{E}_K^{\mathrm{HG}}$, $K \in \mathcal{T}_h$, let $\mathcal{N}_{h,\Gamma}^{\mathrm{HG,N}}$ denote an index set of hanging nodes on Γ that are not associated with a Lagrange basis of order p_Γ on that face. Set $\mathcal{N}_h^{\mathrm{HG,N}} := \bigcup\{\mathcal{N}_{h,\Gamma}^{\mathrm{HG,N}}; \Gamma \in \mathcal{E}_K^{\mathrm{HG}}, K \in \mathcal{T}_h\}$. Let $\mathcal{N}_{h,\Gamma}^{\mathrm{I}}$ and $\mathcal{N}_{h,\Gamma}^{\mathrm{B}}$ be an index set of points on Γ associated with a Lagrange basis of order p_Γ excluding indices from $\mathcal{N}_h^{\mathrm{HG,N}}$ for $\Gamma \in \mathcal{E}_K^{\mathrm{HG,N}} \cup \mathcal{E}_K^{\mathrm{HG}}$, $K \in \mathcal{T}_h$, and $\Gamma \in \mathcal{F}_h^{\mathrm{B}}$, respectively. Further, let $\mathcal{N}_{h,K}^{\circ}$ be an index set of points associated with a Lagrange basis of order $\widetilde{p}_K := \max\{p_\Gamma; \Gamma \in \{\{\mathcal{E}_K^{\mathrm{HG,N}} \cup \mathcal{E}_K^{\mathrm{HG}}\} \bigcup \{\Gamma'; \Gamma'' \subset \Gamma', \Gamma'' \in \mathcal{E}_K\}\}\}$ that lie in the interior of an

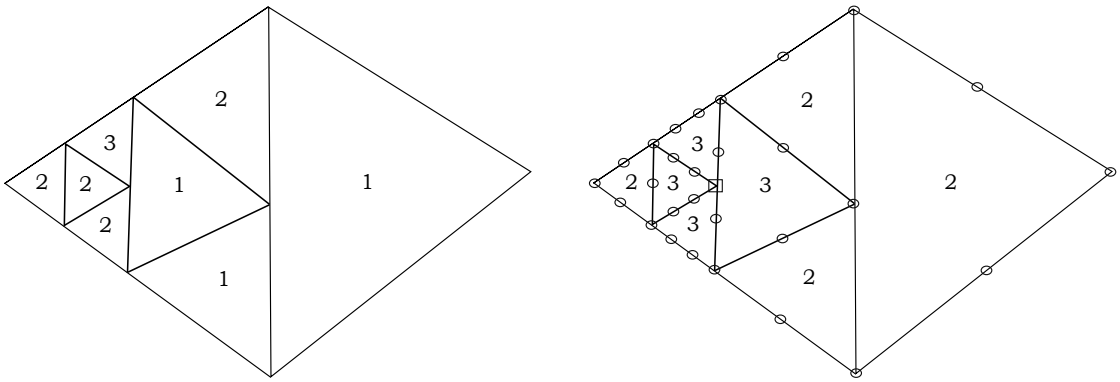

Figure 3: Example of a mesh having variable polynomial degree of the approximate solution u_h^i (left), polynomial degree of $\mathcal{I}_{\mathrm{Av}}(u_h^i)$ in the interior of mesh elements (right), members of the set $\mathcal{N}_h^{\mathrm{HG,N}}$ (square marks) and of the set $\bigcup\{\mathcal{N}_{h,\Gamma}^{\mathrm{I}} \cup \mathcal{N}_{h,\Gamma}^{\mathrm{B}};\, \Gamma \in \mathcal{E}_K^{\mathrm{HG,N}} \cup \mathcal{E}_K^{\mathrm{HG}} \cup \mathcal{F}_h^{\mathrm{B}}\}$ (circle marks) (right).

element K. We will also use the notation $\mathcal{T}_V := \{K \in \mathcal{T}_h; V \in K\}$ for any Lagrangian vertex V (i.e. any point associated with a Lagrange basis in question).

The averaging interpolation operator $\mathcal{I}_{\mathrm{Av}}$ is defined as follows: For all $K \in \mathcal{T}_h$ and $\Gamma \in \mathcal{E}_K^{\mathrm{HG,N}} \cup \mathcal{E}_K^{\mathrm{HG}} \cup \mathcal{F}_h^{\mathrm{B}}$

$$\mathcal{I}_{\mathrm{Av}}(v_h)(V_j) = \begin{cases} \dfrac{1}{\mathrm{card}(\mathcal{T}_{V_j})} \displaystyle\sum_{K' \in \mathcal{T}_{V_j}} v_h|_{K'}(V_j), & j \in \mathcal{N}_{h,\Gamma}^{\mathrm{I}} \cup \mathcal{N}_{h,K}^{\circ}, \\ 0, & j \in \mathcal{N}_{h,\Gamma}^{\mathrm{B}}. \end{cases} \tag{3.1}$$

For elements with a face being a part of a face with a hanging node of the neighboring element, the value from this neighboring element is taken to maintain $H_0^1(\Omega)$-conformity.

We are left with specifying the degrees of freedom from the set $\mathcal{N}_h^{\mathrm{HG,N}}$. Let $K \in \mathcal{T}_h$ possessing a hanging node V_k, $k \in \mathcal{N}_h^{\mathrm{HG,N}}$, be given. Define $\mathcal{Z}_K := \mathcal{N}_{h,K}^{\circ} \bigcup\{\bigcup\{\mathcal{N}_{h,\Gamma}^{\mathrm{I}} \cup \mathcal{N}_{h,\Gamma}^{\mathrm{B}}; \Gamma \in \mathcal{E}_K^{\mathrm{HG,N}} \cup \mathcal{E}_K^{\mathrm{HG}}\}\}$. The value in V_k is then given by extrapolating the value from the inside of K by

$$\mathcal{I}_{\mathrm{Av}}(v_h)(V_k) = \sum_{j \in \mathcal{Z}_K} \left(\frac{1}{\mathrm{card}(\mathcal{T}_{V_j})} \sum_{K' \in \mathcal{T}_{V_j}} v_h|_{K'}(V_j) \right) \varphi_j(V_k), \quad k \in \mathcal{N}_h^{\mathrm{HG,N}}, \tag{3.2}$$

where V_j, $j \in \mathcal{Z}_K$, are the Lagrangian vertices of the element K and the corresponding basis functions φ_j, $j \in \mathcal{Z}_K$, are ordered as the Lagrangian vertices. As above, in other elements possessing the node V_k, the same value is used to maintain $H_0^1(\Omega)$-conformity. Obviously, the polynomial interpolation as defined above does not belong to $S_h^{\boldsymbol{p}}$.

The main reason for such a construction is that we wanted to exploit the advantage of DGMs allowing for easy treatment of nonmatching meshes. In [2, 3] $H_0^1(\Omega)$-conforming interpolation operator is constructed on a sufficiently refined submesh of the original mesh. More precisely, every element $K \in \mathcal{T}_h$ possessing (a) hanging node(s) is uniformly refined to ensure that every hanging node is a vertex of some triangle of the resulting refinement of K. This leads to very fine submeshes in regions where more hanging nodes per edge are present and as such it goes opposite to the intention of using nonmatching meshes. Therefore, no matching submesh of the original mesh is required in our construction.

3.2 Discretization flux reconstruction

Our a posteriori error estimates will be based on equilibrated flux reconstructions (cf. [18, 1, 11]). Let $\boldsymbol{l} = \{l_K\}_{K \in \mathcal{T}_h}$, $\boldsymbol{l} = \boldsymbol{p}$ or $\boldsymbol{l} = \boldsymbol{p} - \mathbf{1}$, where $\boldsymbol{p} - \mathbf{1} = \{p_K - 1\}_{K \in \mathcal{T}_h}$. Let $\mathbf{RTN}_{l_K}(K) := [\mathbb{P}^{l_K}(K)]^d + \mathbf{x}\mathbb{P}^{l_K}(K)$ for $K \in \mathcal{T}_h$. Our reconstructions will be constructed in the broken Raviart–Thomas–Nédélec space

$$\mathbf{RTN}_{\boldsymbol{l}}(\mathcal{T}_h) := \{\mathbf{v}_h \in [L^2(\Omega)]^d, \mathbf{v}_h|_K \in \mathbf{RTN}_{l_K}(K) \quad \forall K \in \mathcal{T}_h\}. \tag{3.3}$$

We thus use for the reconstruction on each mesh element the same or lower-by-one order as for the approximate solution u_h^i. Recall that for $\mathbf{v}_h \in \mathbf{RTN_l}(\mathcal{T}_h)$, we have $\nabla{\cdot}\mathbf{v}_h|_K \in \mathbb{P}^{l_K}(K)$ and $\mathbf{v}_h{\cdot}\mathbf{n}|_\Gamma \in \mathbb{P}^{l_K}(\Gamma)$, $\Gamma \in \mathcal{E}_K$, see [8] or [23].

In our construction, $\mathbf{H}(\mathrm{div}, \Omega)$-conformity of the discretization flux reconstruction may be violated, i.e., $[\mathbf{v}_h{\cdot}\mathbf{n}_\Gamma]_\Gamma \neq 0$ can occur. This violating gives rise to the presence of additional estimators measuring the discontinuity of the normal components of the reconstructed fluxes in our estimates. It happens in two cases:

1. The polynomial degree of the approximate solution in two neighboring elements is different. We could maintain $\mathbf{H}(\mathrm{div}, \Omega)$-conformity in this case by increasing the polynomial degree $\boldsymbol{l}$. However, we prefer to exploit the advantage of DGMs, namely the possibility of varying polynomial degrees, without any extra work for flux reconstructions.

2. The mesh $\mathcal{T}_h$ contains hanging nodes. We could maintain $\mathbf{H}(\mathrm{div}, \Omega)$-conformity in this case by introducing a matching simplicial submesh as in [12, 13, 2, 3]. We, however, want to exploit the advantage of DGMs, namely the simple treatment of hanging nodes, without any extra work for flux reconstructions.

We will construct separately a *discretization flux reconstruction* $\mathbf{d}_h^i$ and an *algebraic error flux reconstruction* $\mathbf{a}_h^i$. The first one is prescibed as follows:

Definition 3.1 (Discretization flux reconstruction)**.** *Let u_h^i solve (2.10). The* discretization flux reconstruction $\mathbf{d}_h^i \in \mathbf{RTN_l}(\mathcal{T}_h)$ *is defined as follows: For all $K \in \mathcal{T}_h$, all $\Gamma \in \mathcal{E}_K$, and all $q_h \in \mathbb{P}^{l_K}(\Gamma)$, we set*

$$(\mathbf{d}_h^i{\cdot}\mathbf{n}_\Gamma, q_h)_\Gamma := (-\langle \nabla u_h^i{\cdot}\mathbf{n}_\Gamma\rangle + \alpha h^{-1}[u_h^i], q_h)_\Gamma, \tag{3.4a}$$

and for all $\mathbf{q}_h \in [\mathbb{P}^{l_K-1}(K)]^d$, we set

$$(\mathbf{d}_h^i, \mathbf{q}_h)_K := (-\nabla u_h^i, \mathbf{q}_h)_K + \theta \sum_{\Gamma\in\mathcal{E}_K} w_\Gamma(\mathbf{q}_h{\cdot}\mathbf{n}_\Gamma, [u_h^i])_\Gamma, \tag{3.4b}$$

where $w_\Gamma := \frac{1}{2}$ for interior faces and $w_\Gamma := 1$ for boundary faces, the function $\alpha : \mathcal{F}_h \to \mathbb{R}$ is defined piecewise by $\alpha|_\gamma := \alpha_\gamma$ for $\gamma \subseteq \Gamma \in \mathcal{E}_K, K \in \mathcal{T}_h$, and the function $h : \mathcal{F}_h \to \mathbb{R}$ is defined by $h|_\gamma := h_\gamma$ for $\gamma \subseteq \Gamma \in \mathcal{E}_K, K \in \mathcal{T}_h$. The values α_γ and h_γ, $\gamma \in \mathcal{F}_h$, were introduced in (2.6a).

The reconstruction $\mathbf{d}_h^i$ has the following property:

Lemma 3.2. *Let $K \in \mathcal{T}_h$ be arbitrary and $\mathbf{d}_h^i$ be given by (3.4). Then*

$$\nabla{\cdot}\mathbf{d}_h^i|_K = \Pi_{l_K}(f|_K - r_h^i|_K),$$

where Π_{l_K} is the L^2-orthogonal projection onto polynomials of degree l_K.

Proof. Let $v_h \in S_h^{\boldsymbol{l}}$, with support on K only, be arbitrary. Using the Green theorem, Definition 3.1, (2.6), and (2.10), we obtain the sequence of equalities

$$(\nabla{\cdot}\mathbf{d}_h^i, v_h)_K = -(\mathbf{d}_h^i, \nabla v_h)_K + \sum_{\Gamma\in\mathcal{E}_K} (\mathbf{d}_h^i{\cdot}\mathbf{n}_K, v_h)_\Gamma = a(u_h^i, v_h) = (f, v_h)_K - (r_h^i, v_h)_K.$$

□

3.3 Algebraic error flux reconstruction

The algebraic error will be measured using the algebraic error flux reconstruction. We follow the recent work [14].

Definition 3.3 (Algebraic error flux reconstruction)**.** *Consider the i-th step of the iterative algebraic solver, leading to (2.9) and (2.10). Perform additional ν steps of the algebraic solver. This gives (2.9) and (2.10) with i replaced by $i+\nu$. Let $\mathbf{d}_h^i$ and $\mathbf{d}_h^{i+\nu}$ be the discretization flux reconstructions given by Definition 3.1, with i replaced by $i+\nu$ in the second case. Then, we define the* algebraic error flux reconstruction *by*

$$\mathbf{a}_h^i := \mathbf{d}_h^{i+\nu} - \mathbf{d}_h^i. \tag{3.5}$$

Due to Definition 3.3, we have immediately for all $K \in \mathcal{T}_h$

$$\nabla{\cdot}\mathbf{a}_h^i|_K = \begin{cases} \nabla{\cdot}\mathbf{d}_h^{i+\nu}|_K - \nabla{\cdot}\mathbf{d}_h^i|_K = \Pi_{p_K} f|_K - r_h^{i+\nu}|_K - \Pi_{p_K} f|_K + r_h^i|_K \\ \qquad\qquad = r_h^i|_K - r_h^{i+\nu}|_K & \text{for } \boldsymbol{l} = \boldsymbol{p}, \\ \Pi_{l_K}(r_h^i|_K - r_h^{i+\nu}|_K) & \text{for } \boldsymbol{l} = \boldsymbol{p}-\mathbf{1}. \end{cases}$$

Let us finally define the *total flux reconstruction* as the sum of the discretization and the algebraic error flux reconstruction,

$$\mathbf{t}_h^i := \mathbf{d}_h^i + \mathbf{a}_h^i. \tag{3.6}$$

Then we have

$$\nabla{\cdot}\mathbf{t}_h^i|_K = \Pi_{l_K}(f|_K - r_h^{i+\nu}|_K) \qquad \forall K \in \mathcal{T}_h,\, \boldsymbol{l} \in \{\boldsymbol{p}-\mathbf{1}, \boldsymbol{p}\}. \tag{3.7}$$

Remark 3.4. *In [15, Section 7.3], another method for construction of the algebraic error flux reconstruction has been proposed. It is more precise, leading to the exact equilibration* $\nabla{\cdot}\mathbf{t}_h^i|_K = \Pi_{l_K} f|_K$ *instead of* (3.7)*, but is more costly. On the contrary, in the present approach, the algebraic error flux reconstruction is constructed simply by* (3.5)*, while the information gained by performing some additional steps of the algebraic solver is used in the next algebraic solver iteration.*

3.4 Guaranteed and fully computable a posteriori error estimate

In the sequel we will use the following inequalities: The Poincaré inequality reads

$$\forall K \in \mathcal{T}_h, \quad \|\varphi - \varphi_K\|_K \le \frac{h_K}{\pi}\|\nabla\varphi\|_K \qquad \forall \varphi \in H^1(K), \tag{3.8}$$

where φ_K denotes the mean value of φ in K. The Friedrichs inequality reads

$$\|\varphi\| \le C_{\mathrm{F},\Omega}\|\nabla\varphi\| \qquad \forall \varphi \in H_0^1(\Omega). \tag{3.9}$$

The constant $C_{\mathrm{F},\Omega}$ can be estimated in the following way, see [25]:

$$C_{\mathrm{F},\Omega} \le \frac{1}{\pi}\left(\frac{1}{a_1} + \ldots + \frac{1}{a_d}\right)^{-\frac{1}{2}}, \tag{3.10}$$

where $a_i, i = 1 \ldots d$, are the lengths of the edges of a cuboid in which the domain Ω is contained. We will also use the trace inequality

$$\forall K \in \mathcal{T}_h,\, \Gamma \in \mathcal{E}_K, \quad \|\varphi - \varphi_\Gamma\|_\Gamma \le C_{\Gamma,K} h_\Gamma^{\frac{1}{2}} \|\nabla\varphi\|_K \qquad \forall \varphi \in H^1(K), \tag{3.11}$$

where φ_Γ denotes the mean value of the trace of φ on Γ. The constant $C_{\Gamma,K}$ has been estimated in [21, Lemma 3.5] as follows:

$$C_{\Gamma,K} \le \left(C_{\mathrm{s},d}\frac{|\Gamma| h_K^2}{|K| h_\Gamma}\right)^{\frac{1}{2}},$$

where $C_{\mathrm{s},d} \approx 0,77708$ for a triangle and $C_{\mathrm{s},d} \approx 3,34055$ for a tetrahedron.

Now, we are ready to state the main theorem concerning the error upper bound. First, we define different error estimators. Consider an i-th iteration step of the algebraic solver. For an arbitrary $K \in \mathcal{T}_h$ we define

$$H_0^1(\Omega)\text{-nonconformity estimator:} \qquad \eta_{\mathrm{NC},K}^i := \|\nabla(u_h^i - \mathcal{I}_{\mathrm{Av}}(u_h^i))\|_K, \tag{3.12a}$$

$$\text{residual estimator:} \qquad \eta_{\mathrm{R},K}^i := \frac{h_K}{\pi}\|f - \nabla{\cdot}\mathbf{t}_h^i - r_h^{i+\nu}\|_K, \tag{3.12b}$$

$$\mathbf{H}(\mathrm{div},\Omega)\text{-nonconformity estimator:} \qquad \eta_{\mathrm{FNC},K}^i := \sum_{\Gamma\in\mathcal{E}_K^{\mathrm{HG}}} C_{\Gamma,K} h_\Gamma^{\frac{1}{2}} \|[\mathbf{t}_h^i{\cdot}\mathbf{n}_\Gamma]\|_\Gamma \tag{3.12c}$$

$$+ \sum_{\Gamma\in\mathcal{E}_K^{\mathrm{HG,N}}} w_\Gamma C_{\Gamma,K} h_\Gamma^{\frac{1}{2}} \|[\mathbf{t}_h^i{\cdot}\mathbf{n}_\Gamma]\|_\Gamma,$$

$$\text{flux estimator:} \qquad \eta_{\mathrm{F},K}^i := \|\nabla u_h^i + \mathbf{t}_h^i\|_K, \tag{3.12d}$$

$$\text{algebraic remainder estimator:} \qquad \eta_{\mathrm{rem},K}^i := C_{\mathrm{F},\Omega}\|r_h^{i+\nu}\|_K, \tag{3.12e}$$

where, we recall, $w_\Gamma = \frac{1}{2}$ for interior faces and $w_\Gamma = 1$ for boundary faces.

Remark 3.5. *Let us point out that the constant $C_{\mathrm{F},\Omega}$ in (3.12e) can be quite large, scaling like h_Ω for regularly-shaped domains Ω, see (3.10). It, however, only appears in the algebraic remainder estimator, which will be made small enough (see Section 4).*

Theorem 3.6 (Guaranteed and fully computable a posteriori error estimate)**.** *Let $u \in H^1_0(\Omega)$ be the weak solution given by (2.1). Let an i-th algebraic solver step be given and let $u_h^i \in S_h^{\boldsymbol{p}}$ be the DGM output given by (2.10). Consider $\nu > 0$ additional algebraic solver steps and let $\mathbf{t}_h^i$ be the total flux reconstruction given by (3.6). Then*

$$\begin{aligned}\|\nabla_h(u-u_h^i)\| &\le \left\{\sum_{K\in\mathcal{T}_h}(\eta^i_{\mathrm{PNC},K})^2 + \left\{\left\{\sum_{K\in\mathcal{T}_h}\left(\eta^i_{\mathrm{R},K}+\eta^i_{\mathrm{F},K}+\eta^i_{\mathrm{FNC},K}\right)^2\right\}^{\frac12} + \left\{\sum_{K\in\mathcal{T}_h}(\eta^i_{\mathrm{rem},K})^2\right\}^{\frac12}\right\}^2\right\}^{\frac12}\\ &=: \eta^i. \end{aligned} \tag{3.13}$$

In order to prove Theorem 3.6, we recall the abstract energy error estimate (see [17, Lemma 4.4]):

Lemma 3.7 (Abstract energy norm estimate)**.** *Let u be the solution of (2.1) and let $u_h \in H^1(\Omega,\mathcal{T}_h)$ be arbitrary. Then*

$$\|\nabla_h(u-u_h)\|^2 \le \inf_{s\in H^1_0(\Omega)}\|\nabla_h(u_h-s)\|^2 + \sup_{\varphi\in H^1_0(\Omega),\|\nabla\varphi\|=1}(\nabla_h(u-u_h),\nabla\varphi)^2. \tag{3.14}$$

Proof of Theorem 3.6. Using $u_h := u_h^i$, $s := \mathcal{I}_{\mathrm{Av}}(u_h^i)$ in (3.14) together with (2.1) gives

$$\|\nabla_h(u-u_h^i)\|^2 \le \|\nabla_h(u_h^i-\mathcal{I}_{\mathrm{Av}}(u_h^i))\|^2 + \sup_{\varphi\in H^1_0(\Omega),\|\nabla\varphi\|=1}\left\{\sum_{K\in\mathcal{T}_h}\{(f,\varphi)_K-(\nabla u_h^i,\nabla\varphi)_K\}\right\}^2. \tag{3.15}$$

Add and subtract $\{(\mathbf{t}_h^i,\nabla\varphi)_K+(r_h^{i+\nu},\varphi)_K\}$ in (3.15) and employ the Green theorem on each $K\in\mathcal{T}_h$ to obtain

$$\begin{aligned}\|\nabla_h(u-u_h^i)\|^2 \le \|\nabla_h(u_h^i-\mathcal{I}_{\mathrm{Av}}(u_h^i))\|^2 + \sup_{\varphi\in H^1_0(\Omega),\|\nabla\varphi\|=1}\Bigg\{\sum_{K\in\mathcal{T}_h}\{&(f-\nabla\cdot\mathbf{t}_h^i-r_h^{i+\nu},\varphi)_K\\ &+(\mathbf{t}_h^i\cdot\mathbf{n}_K,\varphi)_{\partial K}+(r_h^{i+\nu},\varphi)_K-(\nabla u_h^i+\mathbf{t}_h^i,\nabla\varphi)_K\}\Bigg\}^2.\end{aligned} \tag{3.16}$$

Let us estimate the terms in (3.16) separately.

Using (3.7), the Cauchy–Schwarz inequality, the Poincaré inequality (3.8), (3.12b), and (3.12d) gives

$$\begin{aligned}&|(f-\nabla\cdot\mathbf{t}_h^i-r_h^{i+\nu},\varphi)_K-(\nabla u_h^i+\mathbf{t}_h^i,\nabla\varphi)_K| \le \|f-\nabla\cdot\mathbf{t}_h^i-r_h^{i+\nu}\|_K\|\varphi-\varphi_K\|_K+\|\nabla u_h^i+\mathbf{t}_h^i\|_K\|\nabla\varphi\|_K\\ &\le \|f-\nabla\cdot\mathbf{t}_h^i-r_h^{i+\nu}\|_K\frac{h_K}{\pi}\|\nabla\varphi\|_K+\|\nabla u_h^i+\mathbf{t}_h^i\|_K\|\nabla\varphi\|_K = (\eta^i_{\mathrm{R},K}+\eta^i_{\mathrm{F},K})\|\nabla\varphi\|_K.\end{aligned} \tag{3.17}$$

Applying the Cauchy–Schwarz inequality, the Friedrichs inequality (3.9), and (3.12e) yields

$$\sum_{K\in\mathcal{T}_h}(r_h^{i+\nu},\varphi)_K \le \|r_h^{i+\nu}\|\|\varphi\| \le \|r_h^{i+\nu}\|C_{\mathrm{F},\Omega}\|\nabla\varphi\| = \left\{\sum_{K\in\mathcal{T}_h}(\eta^i_{\mathrm{rem},K})^2\right\}^{\frac12}\|\nabla\varphi\|. \tag{3.18}$$

Finally, using (2.4), the fact that $\varphi\in H^1_0(\Omega)$, that $([\mathbf{t}_h^i\cdot\mathbf{n}_\Gamma],\varphi_\Gamma)_\Gamma = 0$ for $\Gamma\in\mathcal{E}_K^{\mathrm{HG}}\cup\mathcal{E}_K^{\mathrm{HG,N}}$, $K\in\mathcal{T}_h$, see (3.4a) and (3.6), and that $([\mathbf{t}_h^i\cdot\mathbf{n}_\Gamma],\varphi)_\Gamma = 0$ for $\Gamma\in\mathcal{E}_K\cap\mathcal{F}_h^{\mathrm{B}}$, we can write,

$$\begin{aligned}\sum_{K\in\mathcal{T}_h}(\mathbf{t}_h^i\cdot\mathbf{n}_K,\varphi)_{\partial K} &= \sum_{K\in\mathcal{T}_h}\left(\sum_{\Gamma\in\mathcal{E}_K^{\mathrm{HG}}}([\mathbf{t}_h^i\cdot\mathbf{n}_\Gamma],\varphi)_\Gamma+\sum_{\Gamma\in\mathcal{E}_K^{\mathrm{HG,N}}}w_\Gamma([\mathbf{t}_h^i\cdot\mathbf{n}_\Gamma],\varphi)_\Gamma\right)\\ &= \sum_{K\in\mathcal{T}_h}\left(\sum_{\Gamma\in\mathcal{E}_K^{\mathrm{HG}}}([\mathbf{t}_h^i\cdot\mathbf{n}_\Gamma],\varphi-\varphi_\Gamma)_\Gamma+\sum_{\Gamma\in\mathcal{E}_K^{\mathrm{HG,N}}}w_\Gamma([\mathbf{t}_h^i\cdot\mathbf{n}_\Gamma],\varphi-\varphi_\Gamma)_\Gamma\right).\end{aligned}$$

Further, using the Cauchy–Schwarz inequality, the trace inequality (3.11), and (3.12c), we obtain

$$\sum_{K\in\mathcal{T}_h}(\mathbf{t}_h^i\cdot\mathbf{n}_K,\varphi)_{\partial K}\le\sum_{K\in\mathcal{T}_h}\left\{\sum_{\Gamma\in\mathcal{E}_K^{\mathrm{HG}}}C_{\Gamma,K}h_\Gamma^{\frac12}\|[\mathbf{t}_h^i\cdot\mathbf{n}_\Gamma]\|_\Gamma\|\nabla\varphi\|_K+\sum_{\Gamma\in\mathcal{E}_K^{\mathrm{HG,N}}}w_\Gamma C_{\Gamma,K}h_\Gamma^{\frac12}\|[\mathbf{t}_h^i\cdot\mathbf{n}_\Gamma]\|_\Gamma\|\nabla\varphi\|_K\right\}$$
$$=\sum_{K\in\mathcal{T}_h}\eta_{\mathrm{FNC},K}^i\|\nabla\varphi\|_K. \tag{3.19}$$

Now, by using (3.17), (3.18), and (3.19) in (3.16) together with the Cauchy–Schwarz inequality, we conclude (3.13). □

Let us now distinguish the discretization and algebraic error components:

$$\text{discretization estimator:}\qquad \eta_{\mathrm{disc},K}^i:=\eta_{\mathrm{PNC},K}^i+\eta_{\mathrm{R},K}^i+\eta_{\mathrm{FD},K}^i+\eta_{\mathrm{FNCD},K}^i, \tag{3.20a}$$
$$\text{algebraic estimator:}\qquad \eta_{\mathrm{alg},K}^i:=\eta_{\mathrm{FA},K}^i+\eta_{\mathrm{FNCA},K}^i, \tag{3.20b}$$

where

$$\eta_{\mathrm{FD},K}^i:=\|\nabla u_h^i+\mathbf{d}_h^i\|_K,\qquad \eta_{\mathrm{FA},K}^i:=\|\mathbf{a}_h^i\|_K,$$
$$\eta_{\mathrm{FNCD},K}^i:=\sum_{\Gamma\in\mathcal{E}_K^{\mathrm{HG}}}C_{\Gamma,K}h_\Gamma^{\frac12}\|[\mathbf{d}_h^i\cdot\mathbf{n}_\Gamma]\|_\Gamma+\sum_{\Gamma\in\mathcal{E}_K^{\mathrm{HG,N}}}w_\Gamma C_{\Gamma,K}h_\Gamma^{\frac12}\|[\mathbf{d}_h^i\cdot\mathbf{n}_\Gamma]\|_\Gamma, \tag{3.21}$$
$$\eta_{\mathrm{FNCA},K}^i:=\sum_{\Gamma\in\mathcal{E}_K^{\mathrm{HG}}}C_{\Gamma,K}h_\Gamma^{\frac12}\|[\mathbf{a}_h^i\cdot\mathbf{n}_\Gamma]\|_\Gamma+\sum_{\Gamma\in\mathcal{E}_K^{\mathrm{HG,N}}}w_\Gamma C_{\Gamma,K}h_\Gamma^{\frac12}\|[\mathbf{a}_h^i\cdot\mathbf{n}_\Gamma]\|_\Gamma.$$

Corollary 3.8 (A posteriori error estimate distinguishing contributions of the discretization and algebraic error)**.** *Let the assumptions of Theorem 3.6 be satisfied. Then*

$$\|\nabla_h(u-u_h^i)\|\le\left\{2\sum_{K\in\mathcal{T}_h}(\eta_{\mathrm{disc},K}^i)^2\right\}^{\frac12}+\left\{\sum_{K\in\mathcal{T}_h}(\eta_{\mathrm{alg},K}^i)^2\right\}^{\frac12}+\left\{\sum_{K\in\mathcal{T}_h}(\eta_{\mathrm{rem},K}^i)^2\right\}^{\frac12}. \tag{3.22}$$

Proof. Using the inequalities $\|\nabla u_h^i+\mathbf{t}_h^i\|_K\le\|\nabla u_h^i+\mathbf{d}_h^i\|_K+\|\mathbf{a}_h^i\|_K$ and $\|[\mathbf{t}_h^i\cdot\mathbf{n}_\Gamma]\|_\Gamma\le\|[\mathbf{d}_h^i\cdot\mathbf{n}_\Gamma]\|_\Gamma+\|[\mathbf{a}_h^i\cdot\mathbf{n}_\Gamma]\|_\Gamma$ following from (3.6), the Cauchy–Schwarz inequality, (3.20) and (3.21), we obtain from (3.13) the assertion (3.22). □

4 Stopping criteria and the adaptive algorithm

We propose in this section our stopping criteria and the corresponding adaptive solution algorithm. As discussed in [15, 14], on a given mesh, there is no need to continue iterations of the algebraic solver when the algebraic error falls below the discretization error. The total error cannot be reduced anyway. Combining this concept with that of adaptive mesh refinement, we propose the following *adaptive solution algorithm*: Let parameters $\gamma_{\mathrm{rem}}>0$, $\gamma_{\mathrm{alg}}>0$, and an integer $\nu^*>0$ be given. Let $\mathcal{T}_1$ be an initial mesh, $U_1^0\in\mathbb{R}^N$ an initial guess for the iterative algebraic solver, and TOL a user-given tolerance (the subscript h from previous sections is in this section replaced by j).

Algorithm 4.1 (Adaptive solution algorithm)**.**

1. *Set* $j:=1$.
2. (a) *Set* $i:=\nu^*$.
   (b) *Perform* ν^* *steps of the algebraic solver starting with* U_j^0 *to get a new approximation* U_j^i *solving (2.9).*
   (c) i. *Set* $\nu:=\nu^*$.
   ii. *Perform* ν^* *additional steps of the algebraic solver starting with* $U_j^{i+\nu-\nu^*}$*, save* $U_j^{i+\nu}$*. Construct new* $\mathbf{a}_j^i$ *following (3.5) and evaluate the estimators* $\eta_{\mathrm{disc},K}^i$*,* $\eta_{\mathrm{alg},K}^i$*, and* $\eta_{\mathrm{rem},K}^i$ *for all* $K\in\mathcal{T}_j$.

iii. Check whether

$$\eta^i_{\mathrm{rem},K} \le \gamma_{\mathrm{rem}}(\eta^i_{\mathrm{disc},K} + \eta^i_{\mathrm{alg},K}) \qquad \forall K \in \mathcal{T}_j. \tag{4.1a}$$

If not satisfied, set $\nu := \nu + \nu^*$ and go back to step 2(c)ii.

(d) Check whether

$$\eta^i_{\mathrm{alg},K} \le \gamma_{\mathrm{alg}} \eta^i_{\mathrm{disc},K} \qquad \forall K \in \mathcal{T}_j. \tag{4.1b}$$

If not satisfied, $i := i + \nu$ and go to step 2(c)i.

3. Check whether $\eta^i \le TOL$. If satisfied, stop. Else refine $\mathcal{T}_j$ adaptively to $\mathcal{T}_{j+1}$, interpolate the currently available U^i_j from $\mathcal{T}_j$ to $\mathcal{T}_{j+1}$ to get new U^0_{j+1}, set $j := j + 1$, and go to step 2a.

Remark 4.2 (Global stopping criteria)**.** *One can also define the following global version of the criteria (4.1):*

$$\eta^i_{\mathrm{rem}} \le \gamma_{\mathrm{rem}}(\eta^i_{\mathrm{disc}} + \eta^i_{\mathrm{alg}}), \tag{4.2a}$$

$$\eta^i_{\mathrm{alg}} \le \gamma_{\mathrm{alg}} \eta^i_{\mathrm{disc}}, \tag{4.2b}$$

where $\eta^i_{\mathrm{rem}} := \left\{\sum_{K\in\mathcal{T}_h} (\eta^i_{\mathrm{rem},K})^2\right\}^{\frac{1}{2}}$, $\eta^i_{\mathrm{alg}} := \left\{\sum_{K\in\mathcal{T}_h} (\eta^i_{\mathrm{alg},K})^2\right\}^{\frac{1}{2}}$, $\eta^i_{\mathrm{disc}} := \left\{\sum_{K\in\mathcal{T}_h} (\eta^i_{\mathrm{disc},K})^2\right\}^{\frac{1}{2}}$.

5 Local efficiency of the a posteriori error estimate

In this section, we will show that the estimators $\eta^i_{\mathrm{disc},K}$, $\eta^i_{\mathrm{alg},K}$, and $\eta^i_{\mathrm{rem},K}$ also provide local lower bound for the error. This gives a theoretical justification of these estimators and of their usage in Algorithm 4.1. Recall that $\mathcal{T}_K$ denotes the set of the element K itself with its neighbors (including all elements that are contained in the macro-element sharing a complete face with the element K in case K possesses a hanging node), $\mathcal{F}_K$ denotes the faces Γ in this patch, and $\widetilde{\mathcal{F}}_K$ the set of faces γ that share at least a vertex with K.

Theorem 5.1 (Local efficiency of the estimate)**.** *Let $u \in H^1_0(\Omega)$ be the weak solution given by (2.1). Let an i-th algebraic solver step be given and let $u^i_h \in S^{\boldsymbol{p}}_h$ be given by (2.10). Let f be a piecewise polynomial of degree $\boldsymbol{p}$. Let finally the algebraic solver be stopped as soon as the local stopping criteria (4.1) hold. Then there exists a generic constant C depending only on the shape-regularity constant C_{s} of (2.5a), the local quasi-uniformity constant C_H of (2.5b), the given weights γ_{rem} and γ_{alg}, the space dimension d, the DGM penalty parameter $\alpha_{\max} := \max_{\gamma\in\mathcal{F}_h} \alpha_\gamma$, and the polynomial degree $\boldsymbol{p}$ of the function u^i_h such that, for all $K \in \mathcal{T}_h$,*

$$\eta^i_{\mathrm{disc},K} + \eta^i_{\mathrm{alg},K} + \eta^i_{\mathrm{rem},K} \le C \left\{ \sum_{K'\in\mathcal{T}_h; \mathcal{T}_K\cap\mathcal{T}_{K'}\neq\emptyset} \|\nabla(u - u^i_h)\|^2_{K'} \right\}^{\frac{1}{2}} + C \left\{ \sum_{\gamma\in\mathcal{F}_K\cup\widetilde{\mathcal{F}}_K} h_\gamma^{-1} \|[u^i_h]\|^2_\gamma \right\}^{\frac{1}{2}}. \tag{5.1}$$

Proof. Let $K \in \mathcal{T}_h$ be arbitrary but fixed. Due to the imposed local stopping criteria (4.1), we have

$$\eta^i_{\mathrm{disc},K} + \eta^i_{\mathrm{alg},K} + \eta^i_{\mathrm{rem},K} \le C \eta^i_{\mathrm{disc},K}. \tag{5.2}$$

First, analogously to [16], it can be shown that the operator $\mathcal{I}_{\mathrm{Av}}$ defined in Section 3.1 has the following approximation property:

$$\|\nabla(v_h - \mathcal{I}_{\mathrm{Av}}(v_h))\|^2_K \le C \sum_{\gamma\in\widetilde{\mathcal{F}}_K} h_\gamma^{-1} \|[v_h]\|^2_\gamma, \quad \forall v_h \in S^{\boldsymbol{p}}_h.$$

Thus, we have

$$\eta^i_{\mathrm{PNC},K} \le C \left\{ \sum_{\gamma\in\widetilde{\mathcal{F}}_K} h_\gamma^{-1} \|[u^i_h]\|^2_\gamma \right\}^{\frac{1}{2}}. \tag{5.3}$$

Further, observe that if the flux reconstruction $\mathbf{t}_h^i$ has the order $\boldsymbol{l} = \boldsymbol{p}$, $\eta_{\mathrm{R},K}^i = \frac{h_K}{\pi}\|f - \nabla\cdot\mathbf{t}_h^i - r_h^{i+\nu}\|_K = 0$ due to (3.7) and the assumption made on f. In the case of $\boldsymbol{l} = \boldsymbol{p} - \mathbf{1}$ we proceed as follows. By adding and subtracting Δu_h^i in $\eta_{\mathrm{R},K}^i$, using the triangle inequality and the inverse inequality

$$\|\nabla v_h\|_K \le C h_K^{-1}\|v_h\|_K \qquad \forall v_h \in \mathbb{P}^{p_K}(K),$$

we have

$$\eta_{\mathrm{R},K}^i \le \frac{h_K}{\pi}\|f + \Delta u_h^i\|_K + C\|\nabla u_h^i + \mathbf{t}_h^i\|_K + \frac{h_K}{\pi}\|r_h^{i+\nu}\|_K.$$

Further, (3.6) and the triangle inequality give

$$\eta_{\mathrm{R},K}^i \le \frac{h_K}{\pi}\|f + \Delta u_h^i\|_K + C\|\nabla u_h^i + \mathbf{d}_h^i\|_K + C\|\mathbf{a}_h^i\|_K + \frac{h_K}{\pi}\|r_h^{i+\nu}\|_K. \tag{5.4}$$

Due to (3.20b) and (3.12e), the last two terms are bounded by $\eta_{\mathrm{alg},K}^i + \eta_{\mathrm{rem},K}^i$. The first term is a standard residual estimator known to satisfy (see [28])

$$h_K\|f + \Delta u_h^i\|_K \le C\|\nabla(u - u_h^i)\|_K. \tag{5.5}$$

Next, we will estimate $\|\nabla u_h^i + \mathbf{d}_h^i\|_K$. According to [9, Lemma 3.5], we can write

$$\|\nabla u_h^i + \mathbf{d}_h^i\|_K^2 \le C\left\{h_K \sum_{\Gamma\in\mathcal{E}_K}\|(\nabla u_h^i + \mathbf{d}_h^i)\cdot\mathbf{n}_\Gamma\|_\Gamma^2 + \left(\sup_{\mathbf{q}_h\in[\mathbb{P}_{l_K-1}(K)]^d}\frac{(\nabla u_h^i + \mathbf{d}_h^i, \mathbf{q}_h)_K}{\|\mathbf{q}_h\|_K}\right)^2\right\}. \tag{5.6}$$

For $\mathbf{q}_h \in [\mathbb{P}^{l_K-1}(K)]^d$, taking into account definition (3.4b), we have

$$(\nabla u_h^i + \mathbf{d}_h^i, \mathbf{q}_h)_K = \theta\sum_{\Gamma\in\mathcal{E}_K} w_\Gamma(\mathbf{q}_h\cdot\mathbf{n}_\Gamma, [u_h^i])_\Gamma.$$

Now, by using the Cauchy–Schwarz inequality and the inverse inequality $\|\mathbf{q}_h\|_\Gamma \le C h_K^{-1/2}\|\mathbf{q}_h\|_K$, we obtain

$$(\nabla u_h^i + \mathbf{d}_h^i, \mathbf{q}_h)_K \le C|\theta| h_K^{-1/2}\|\mathbf{q}_h\|_K \sum_{\Gamma\in\mathcal{E}_K} w_\Gamma\|[u_h^i]\|_\Gamma. \tag{5.7}$$

By putting (5.7) into (5.6) and using definition (3.4a), we get

$$\|\nabla u_h^i + \mathbf{d}_h^i\|_K^2 \le C\left\{h_K\sum_{\Gamma\in\mathcal{E}_K^{\mathrm{I}}}\|\Pi_{l_K}[\nabla u_h^i\cdot\mathbf{n}_\Gamma]\|_\Gamma^2 + h_K\alpha_{\max}^2\sum_{\Gamma\in\mathcal{E}_K} h_\Gamma^{-2}\|\Pi_{l_K}[u_h^i]\|_\Gamma^2 \right.$$
$$\left. + |\theta|^2 h_K^{-1}\sum_{\Gamma\in\mathcal{E}_K} w_\Gamma^2\|[u_h^i]\|_\Gamma^2\right\}.$$

Let $\Gamma \in \mathcal{E}_K^{\mathrm{I}}$. With the aid of the edge bubble functions technique introduced by Verfürth, see [28], it can be shown that

$$h_\Gamma^{\frac{1}{2}}\|[\nabla u_h^i\cdot\mathbf{n}_\Gamma]\|_\Gamma \le \begin{cases} C\displaystyle\sum_{K''\in\{K_\gamma^{\mathrm{L}}, K_\gamma^{\mathrm{R}}\}}\|\nabla(u - u_h^i)\|_{K''} & \text{for} \quad \gamma = \Gamma \in \mathcal{E}_K^{\mathrm{I}}\setminus\mathcal{E}_K^{\mathrm{HG}}, \\ C\left(\|\nabla(u - u_h^i)\|_K + \displaystyle\sum_{K'\subset K_\Gamma^{\mathrm{NEI}}}\|\nabla(u - u_h^i)\|_{K'}\right) & \text{for} \quad \Gamma \in \mathcal{E}_K^{\mathrm{HG}}, \end{cases}$$

where K_Γ^{NEI} denotes the macro-element sharing the complete face Γ with the element K. Therefore, by taking into account the estimate

$$\|\Pi_{l_K}[\nabla u_h^i\cdot\mathbf{n}_\Gamma]\|_\Gamma \le \|[\nabla u_h^i\cdot\mathbf{n}_\Gamma]\|_\Gamma, \quad \Gamma \in \mathcal{E}_K^{\mathrm{I}}, \tag{5.8}$$

we obtain

$$h_K \sum_{\Gamma\in\mathcal{E}_K^{\mathrm{I}}} \|\Pi_{l_K}[\nabla u_h^i\cdot\mathbf{n}_\Gamma]\|_\Gamma^2 \le h_K \sum_{\Gamma\in\mathcal{E}_K^{\mathrm{I}}} \|[\nabla u_h^i\cdot\mathbf{n}_\Gamma]\|_\Gamma^2 \le C \sum_{K\in\mathcal{T}_K} \|\nabla(u-u_h^i)\|_K^2.$$

Finally, using

$$\|\Pi_{l_K}[u_h^i]\|_\Gamma \le \|[u_h^i]\|_\Gamma$$

yields

$$\|\nabla u_h^i + \mathbf{d}_h^i\|_K^2 \le C\left\{\sum_{K\in\mathcal{T}_K} \|\nabla(u-u_h^i)\|_K^2 + (\alpha_{\max}^2+1)\sum_{\Gamma\in\mathcal{E}_K} h_\Gamma^{-1}\|[u_h^i]\|_\Gamma^2\right\}. \tag{5.9}$$

Now, it remains to estimate the last term of (3.20a). According to the estimate in [29, Theorem 3.3, (3.21)] and [22, Theorem 4.3], for a vector only piecewise in $\mathbf{H}(\mathrm{div},\cdot)$, we can write

$$h_\Gamma^{\frac12}\|[\mathbf{d}_h^i\cdot\mathbf{n}_\Gamma]\|_\Gamma \le \begin{cases} C \displaystyle\sum_{K''\in\{K_\gamma^{\mathrm{L}},K_\gamma^{\mathrm{R}}\}} \|\mathbf{d}_h^i+\nabla u\|_{K''} & \text{for}\quad \gamma=\Gamma\in\mathcal{E}_K^{\mathrm{HG,N}},\\ C\left(\|\mathbf{d}_h^i+\nabla u\|_K + \displaystyle\sum_{K'\subset K_\Gamma^{\mathrm{NEI}}} \|\mathbf{d}_h^i+\nabla u\|_{K'}\right) & \text{for}\quad \Gamma\in\mathcal{E}_K^{\mathrm{HG}}. \end{cases}$$

Now, adding and subtracting ∇u_h^i in the norm to the above right-hand sides together with the triangle inequality yields

$$h_\Gamma^{\frac12}\|[\mathbf{d}_h^i\cdot\mathbf{n}_\Gamma]\|_\Gamma \le \begin{cases} C \displaystyle\sum_{K''\in\{K_\gamma^{\mathrm{L}},K_\gamma^{\mathrm{R}}\}} \big(\|\mathbf{d}_h^i+\nabla u_h^i\|_{K''} + \|\nabla(u-u_h^i)\|_{K''}\big) & \text{for}\quad \gamma=\Gamma\in\mathcal{E}_K^{\mathrm{HG,N}},\\ C\Big(\|\mathbf{d}_h^i+\nabla u_h^i\|_K + \|\nabla(u-u_h^i)\|_K & \\ \quad + \displaystyle\sum_{K'\subset K_\Gamma^{\mathrm{NEI}}} \big(\|\mathbf{d}_h^i+\nabla u_h^i\|_{K'} + \|\nabla(u-u_h^i)\|_{K'}\big)\Big) & \text{for}\quad \Gamma\in\mathcal{E}_K^{\mathrm{HG}}. \end{cases} \tag{5.10}$$

Now combining (5.2) with definition (3.20a) and (5.3), (5.4), (5.5), (5.9), and (5.10) gives

$$\begin{aligned}\eta_{\mathrm{disc},K}^i + \eta_{\mathrm{alg},K}^i + \eta_{\mathrm{rem},K}^i \le{}& C\left\{\sum_{K'\in\mathcal{T}_h;\mathcal{T}_K\cap\mathcal{T}_{K'}\neq\emptyset} \|\nabla(u-u_h^i)\|_{K'}^2\right\}^{\frac12} + C\left\{\sum_{\gamma\in\mathcal{F}_K\cup\widetilde{\mathcal{F}}_K} h_\gamma^{-1}\|[u_h^i]\|_\gamma^2\right\}^{\frac12}\\ &+ C(\eta_{\mathrm{alg},K}^i + \eta_{\mathrm{rem},K}^i).\end{aligned}$$

Choosing γ_{rem} and γ_{alg} in (4.1) small enough allows to discard the contribution of $\eta_{\mathrm{alg},K}^i$ and $\eta_{\mathrm{rem},K}^i$ from the above right-hand side and to arrive at (5.1). □

6 Simple evaluation of the a posteriori estimates

The estimators of Theorem 3.6 and Corollary 3.8 may seem rather difficult to evaluate at a first sight. In particular the flux reconstructions in RTN spaces may be a little involved to code and work with. In this section, we show that, at least for low-order approximations (most frequently used in practice), our estimates lead to simple formulas not featuring the flux reconstructions which are easy to implement and evaluate.

6.1 First-order discretization

We start with the simplest case considering $u_h^i \in S_h^1$ and $\mathbf{t}_h^i \in \mathbf{RTN_0}(\mathcal{T}_h)$. Let us first provide an explicit definition of $\mathbf{RTN_0}(\mathcal{T}_h)$-basis.

Definition 6.1. (Definition of $\mathbf{RTN_0}(\mathcal{T}_h)$-basis functions) *Let a simplex $K \in \mathcal{T}_h$ be given. Let $\Gamma_j, j = 1 \dots d+1$, be its faces/edges and $V_{\Gamma_j}, j = 1 \dots d+1$, the opposite vertices, respectively. Let $\mathbf{n}_{j,\partial K}$ denote the unit outward normal to K along Γ_j. The $\mathbf{RTN_0}(\mathcal{T}_h)$-basis functions are defined by*

$$\boldsymbol{\psi}_{\Gamma_j}(\mathbf{x}) := \mathbf{n}_{\Gamma_j} \cdot \mathbf{n}_{j,\partial K} \frac{1}{d|K|}(\mathbf{x} - V_{\Gamma_j}) \qquad \text{for } j = 1 \dots d+1,\ \mathbf{x} \in K.$$

Notice that the volume $|K|$ can be computed by the formula:

$$|K| = \frac{1}{d!} \det \begin{pmatrix} V_{\Gamma_1} & \dots & V_{\Gamma_{d+1}} \\ 1 & \dots & 1 \end{pmatrix}.$$

For any $\mathbf{t}_h^i \in \mathbf{RTN_0}(\mathcal{T}_h)$, we can write $\mathbf{t}_h^i|_K = \sum_{\Gamma \in \mathcal{E}_K} (\mathbf{t}_h^i)_\Gamma \boldsymbol{\psi}_\Gamma$, where $(\mathbf{t}_h^i)_\Gamma$ are the degrees of freedom associated with the basis of Definition 6.1. Recall that we distinguish the discretization and algebraic components, i.e., $\mathbf{t}_h^i = \mathbf{d}_h^i + \mathbf{a}_h^i$. Let $K \in \mathcal{T}_h$ be fixed. Then, for $\Gamma \in \mathcal{E}_K$, the coefficients $(\mathbf{d}_h^i)_\Gamma$ are given by, see (3.4a),

$$(\mathbf{d}_h^i)_\Gamma := (\mathbf{d}_h^i \cdot \mathbf{n}_\Gamma, 1)_\Gamma = (-\langle \nabla u_h^i \cdot \mathbf{n}_\Gamma \rangle + \alpha h^{-1} [u_h^i], 1)_\Gamma, \tag{6.1a}$$

whereas coefficients $(\mathbf{a}_h^i)_\Gamma$ are given by, see Definition 3.3,

$$(\mathbf{a}_h^i)_\Gamma := ((\mathbf{d}_h^{i+\nu} - \mathbf{d}_h^i) \cdot \mathbf{n}_\Gamma, 1)_\Gamma = (-\langle \nabla (u_h^{i+\nu} - u_h^i) \cdot \mathbf{n}_\Gamma \rangle + \alpha h^{-1} [u_h^{i+\nu} - u_h^i], 1)_\Gamma. \tag{6.1b}$$

Let $\{\varphi_j\}_{j \in \mathcal{S}_K}$ be a basis of $S_h^1|_K$ and $\{\varphi_j\}_{j \in \mathcal{N}_K}$ a basis of S_h^1 on K and all its neighbors. Expressing u_h^i in these bases yields

$$u_h^i|_K = \sum_{j \in \mathcal{S}_K} (u_h^i)_j \varphi_j, \qquad u_h^i|_{K' \in \mathcal{T}_h;\, |\partial K \cap \partial K'| > 0} = \sum_{j \in \mathcal{N}_K} (u_h^i)_j \varphi_j. \tag{6.2}$$

Using (6.2) in (6.1a) and (6.1b) gives

$$(\mathbf{d}_h^i)_\Gamma = (\mathbf{d}_h^i \cdot \mathbf{n}_\Gamma, 1)_\Gamma = \Big(- \sum_{j \in \mathcal{N}_K} (u_h^i)_j \langle \nabla \varphi_j \cdot \mathbf{n}_\Gamma \rangle + \alpha h^{-1} \sum_{j \in \mathcal{N}_K} (u_h^i)_j [\varphi_j], 1 \Big)_\Gamma, \tag{6.3a}$$

$$(\mathbf{a}_h^i)_\Gamma = (\mathbf{a}_h^i \cdot \mathbf{n}_\Gamma, 1)_\Gamma = \Big(- \sum_{j \in \mathcal{N}_K} (u_h^{i+\nu} - u_h^i)_j \langle \nabla \varphi_j \cdot \mathbf{n}_\Gamma \rangle + \alpha h^{-1} \sum_{j \in \mathcal{N}_K} (u_h^{i+\nu} - u_h^i)_j [\varphi_j], 1 \Big)_\Gamma. \tag{6.3b}$$

Now, we are ready to provide explicit formulas for evaluation of a posteriori error estimators in Corollary 3.8 avoiding the physical construction of the potential reconstruction $\mathcal{I}_{\mathrm{Av}}(u_h^i)$ and of the flux reconstructions $\mathbf{d}_h^i$ and $\mathbf{a}_h^i$.

Let us start with the estimator $\|\nabla u_h^i + \mathbf{d}_h^i\|_K$. First, $(\nabla u_h^i + \mathbf{d}_h^i)|_K \in [\mathbb{P}^1(K)]^d$ holds. Thus, we will need a quadrature rule that is exact for quadratic polynomials such as

$$\int_K w(\mathbf{x})\, \mathrm{d}\mathbf{x} \approx \begin{cases} \dfrac{|K|}{3} \displaystyle\sum_{\Gamma \in \mathcal{E}_K} w(\mathbf{x}_\Gamma), & \text{for } d = 2, \\ \dfrac{|K|}{20} \displaystyle\sum_{k=1}^{4} w(V_{\Gamma_k}) + \dfrac{4|K|}{5} w(\mathbf{x}_g), & \text{for } d = 3, \end{cases} \tag{6.4}$$

where $\mathbf{x}_\Gamma$ are the mid-points of the sides of the triangle K whereas $\mathbf{x}_g$ is the barycentre and V_{Γ_k}, $k = 1, 2, 3, 4$, are the vertices of the tetrahedron K. Recall that $\mathcal{E}_K$ denotes the set of the faces of the element K. With

the aid of (6.4) and (6.3a), we have

$$\|\nabla u_h^i + \mathbf{d}_h^i\|_K^2 = \begin{cases} \dfrac{|K|}{3} \displaystyle\sum_{\Gamma\in\mathcal{E}_K} \left| \sum_{j\in\mathcal{S}_K} (u_h^i)_j \nabla\varphi_j(\mathbf{x}_\Gamma) + \sum_{\Gamma'\in\mathcal{E}_K} (\mathbf{d}_h^i)_{\Gamma'} \boldsymbol{\psi}_{\Gamma'}(\mathbf{x}_\Gamma) \right|^2, & \text{for } d=2, \\ \dfrac{|K|}{20} \displaystyle\sum_{k=1}^{4} \left| \sum_{j\in\mathcal{S}_K} (u_h^i)_j \nabla\varphi_j(V_{\Gamma_k}) + \sum_{\Gamma'\in\mathcal{E}_K} (\mathbf{d}_h^i)_{\Gamma'} \boldsymbol{\psi}_{\Gamma'}(V_{\Gamma_k}) \right|^2 \\ \quad + \dfrac{4|K|}{5} \left| \displaystyle\sum_{j\in\mathcal{S}_K} (u_h^i)_j \nabla\varphi_j(\mathbf{x}_g) + \sum_{\Gamma'\in\mathcal{E}_K} (\mathbf{d}_h^i)_{\Gamma'} \boldsymbol{\psi}_{\Gamma'}(\mathbf{x}_g) \right|^2, & \text{for } d=3. \end{cases}$$

Analogously, as $\mathbf{a}_h^i|_K \in [\mathbb{P}^1(K)]^d$, we get

$$\|\mathbf{a}_h^i\|_K^2 = \begin{cases} \dfrac{|K|}{3} \displaystyle\sum_{\Gamma\in\mathcal{E}_K} \left| \sum_{\Gamma'\in\mathcal{E}_K} (\mathbf{a}_h^i)_{\Gamma'} \boldsymbol{\psi}_{\Gamma'}(\mathbf{x}_\Gamma) \right|^2, & \text{for } d=2, \\ \dfrac{|K|}{20} \displaystyle\sum_{k=1}^{4} \left| \sum_{\Gamma'\in\mathcal{E}_K} (\mathbf{a}_h^i)_{\Gamma'} \boldsymbol{\psi}_{\Gamma'}(V_{\Gamma_k}) \right|^2 + \dfrac{4|K|}{5} \left| \displaystyle\sum_{\Gamma'\in\mathcal{E}_K} (\mathbf{a}_h^i)_{\Gamma'} \boldsymbol{\psi}_{\Gamma'}(\mathbf{x}_g) \right|^2, & \text{for } d=3. \end{cases}$$

Another estimator that needs to be evaluated is $\|\nabla(u_h^i - \mathcal{I}_{\mathrm{Av}}(u_h^i))\|_K$. As $\nabla(u_h^i - \mathcal{I}_{\mathrm{Av}}(u_h^i))|_K \in [\mathbb{P}^0(K)]^d$ holds, the following quadrature rule of the algebraic order 1 is sufficient:

$$\int_K w(\mathbf{x})\,\mathrm{d}\mathbf{x} \approx |K| w(\mathbf{x}_g),$$

where $\mathbf{x}_g$ is the barycentre of the simplex K. With the aid of (6.2) and (3.1), we can write

$$\|\nabla(u_h^i - \mathcal{I}_{\mathrm{Av}}(u_h^i))\|_K^2 = |K| \left| \sum_{j\in\mathcal{S}_K} (u_h^i)_j \nabla\varphi_j(\mathbf{x}_g) - \nabla \sum_{k=1}^{d+1} (\mathcal{I}_{\mathrm{Av}}(u_h^i))_k \varphi_k(\mathbf{x}_g) \right|^2,$$

$$(\mathcal{I}_{\mathrm{Av}}(u_h^i))_k := \begin{cases} \dfrac{1}{\mathrm{card}(\mathcal{T}_{V_{\Gamma_k}})} \displaystyle\sum_{K'\in\mathcal{T}_{V_{\Gamma_k}}} \sum_{j\in\mathcal{S}_{K'}} (u_h^i)_j \varphi_j|_{K'}(V_{\Gamma_k}), & \text{for } k \notin \mathcal{N}_h^{\mathrm{HG,N}}, \\ \displaystyle\sum_{j\in\mathcal{Z}_K} \left(\frac{1}{\mathrm{card}(\mathcal{T}_{V_j})} \sum_{K'\in\mathcal{T}_{V_j}} \sum_{l\in\mathcal{S}_{K'}} (u_h^i)_l \varphi_l|_{K'}(V_j) \right) \varphi_j(V_{\Gamma_k}), & \text{for } k \in \mathcal{N}_h^{\mathrm{HG,N}}, \end{cases}$$

where $\mathcal{Z}_K$ is defined below (3.1), V_{Γ_k}, $k = 1 \ldots d+1$, are the vertices of the element K and the basis functions φ_k of $S_h^{\mathbf{1}}|_K$ are ordered as the vertices.

Now, the estimators

$$\sum_{\Gamma\in\mathcal{E}_K^{\mathrm{HG}}} C_{\Gamma,K} h_\Gamma^{\frac{1}{2}} \|[\mathbf{d}_h^i \cdot \mathbf{n}_\Gamma]\|_\Gamma \quad \text{and} \quad \sum_{\Gamma\in\mathcal{E}_K^{\mathrm{HG,N}}} w_\Gamma C_{\Gamma,K} h_\Gamma^{\frac{1}{2}} \|[\mathbf{d}_h^i \cdot \mathbf{n}_\Gamma]\|_\Gamma$$

are to be evaluated. Due to the fact that $[\mathbf{d}_h^i \cdot \mathbf{n}_\Gamma]|_\Gamma \in \mathbb{P}^0(\Gamma)$, it is quite easy. There are two cases to consider:

1. If both the face Γ has no hanging node and the polynomial degrees of the approximate solution u_h^i on the adjacent triangles agree, then
$$[\mathbf{d}_h^i \cdot \mathbf{n}_\Gamma]_\Gamma = 0.$$

2. The face Γ possesses a hanging node or polynomial degrees of the approximate solution u_h^i on the adjacent triangles disagree. For simplicity, let us assume that only one hanging node is present. Let

γ_1 and γ_2 be those parts which have the hanging node in common and which comprise the face Γ. Let K_1 and K_2 be the elements sharing their faces with K (see Fig. 4). Then

$$\begin{aligned}\|[\mathbf{d}_h^i \cdot \mathbf{n}_\Gamma]\|_\Gamma^2 = &\left([-\langle \nabla u_h^i \cdot \mathbf{n}_{\gamma_1}\rangle] + \alpha_{\gamma_1} h_{\gamma_1}^{-1}(\Pi_{0,\gamma_1} - \Pi_{0,\Gamma}|_{\gamma_1})[u_h^i]\right)^2 |\gamma_1| \\ &+ \left([-\langle \nabla u_h^i \cdot \mathbf{n}_{\gamma_2}\rangle] + \alpha_{\gamma_2} h_{\gamma_2}^{-1}(\Pi_{0,\gamma_2} - \Pi_{0,\Gamma}|_{\gamma_2})[u_h^i]\right)^2 |\gamma_2|,\end{aligned}$$

where Π_{0,Γ_j}, $j = 1, 2$, and $\Pi_{0,\Gamma}$ are the L^2-orthogonal projections onto $\mathbb{P}^0(\Gamma_j)$, $j = 1, 2$, and $\mathbb{P}^0(\Gamma)$, respectively.

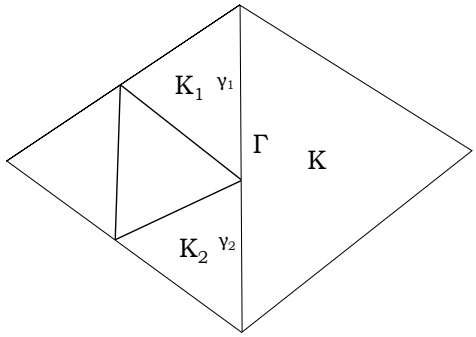

Figure 4: Components of a face Γ

Finally, the second and third terms of (3.20b) remain to be evaluated. But this can be done in the same way as just above.

6.2 Second-order discretization

We continue by considering $u_h^i \in S_h^{\mathbf{2}}$ and $\mathbf{t}_h^i \in \mathbf{RTN_1}(\mathcal{T}_h)$. Let us state the explicit definition of $\mathbf{RTN_1}(\mathcal{T}_h)$-basis.

Definition 6.2. (Definition of $\mathbf{RTN_1}(\mathcal{T}_h)$-basis functions) *Let a simplex $K \in \mathcal{T}_h$ be given. Let $\Gamma_j, j = 1 \dots d+1$, be its faces/edges and $V_{\Gamma_j}, j = 1 \dots d+1$, the opposite vertices, respectively. Let $\mathbf{n}_{j,\partial K}$ denote the unit outward normal to ∂K along Γ_j. Let $\mathbf{e}_j$, $j = 1 \dots d+1$, stand for the canonical basis of $\mathbb{R}^d$ and S_{Γ_j} for the average value of S on Γ_j. Let finally λ_j, $j = 1 \dots d+1$, be the barycentric coordinates, φ_l be the basis functions of $\mathbb{P}^2(K)$ of the type $4\lambda_i\lambda_j$, $1 \le i < j \le d+1$, and $\boldsymbol{\phi}_l$, $l = 1 \dots 8$, be defined by:*

$$\begin{bmatrix} x_2^2 \\ -x_1x_2 \\ 0 \end{bmatrix}, \quad \begin{bmatrix} 0 \\ -x_2x_3 \\ x_2^2 \end{bmatrix}, \quad \begin{bmatrix} -x_1x_2 \\ x_1^2 \\ 0 \end{bmatrix}, \quad \begin{bmatrix} -x_1x_3 \\ 0 \\ x_1^2 \end{bmatrix}, \quad \begin{bmatrix} x_3^2 \\ 0 \\ -x_1x_3 \end{bmatrix}, \quad \begin{bmatrix} 0 \\ x_3^2 \\ -x_2x_3 \end{bmatrix}, \quad \begin{bmatrix} x_2x_3 \\ -x_1x_3 \\ 0 \end{bmatrix}, \quad \begin{bmatrix} 0 \\ x_1x_3 \\ -x_1x_2 \end{bmatrix}.$$

The $\mathbf{RTN_1}(\mathcal{T}_h)$-basis functions corresponding to the following degrees of freedom

$$\begin{aligned} \mathbf{q} &\mapsto \int_{\Gamma_j} \mathbf{q}\cdot\mathbf{n}_{\Gamma_j}\,\mathrm{d}S && \text{for } j = 1 \dots d+1, \\ \mathbf{q} &\mapsto \int_{\Gamma_j} \mathbf{q}\cdot\mathbf{n}_{j,\partial K}(S - S_{\Gamma_j})\,\mathrm{d}S && \text{for } j = 1 \dots d+1, \\ \mathbf{q} &\mapsto \int_K \mathbf{q}\cdot\mathbf{e}_j\,\mathrm{d}\mathbf{x} && \text{for } j = 1 \dots d+1 \end{aligned}$$

are defined as follows

$$\boldsymbol{\psi}_{\Gamma_j}(\mathbf{x}) := \mathbf{n}_{\Gamma_j}\cdot\mathbf{n}_{j,\partial K}\frac{1}{d|K|}(\mathbf{x}-V_{\Gamma_j}) \qquad \text{for } j=1\dots d+1,\ \mathbf{x}\in K,$$

$$\boldsymbol{\psi}_l(\mathbf{x}) := \begin{cases} \mathbf{curl}\varphi_l & \text{for } l=1\dots 3 \quad \text{if } d=2,\\ \mathbf{curl}\boldsymbol{\phi}_l & \text{for } l=1\dots 8 \quad \text{if } d=3,\end{cases}$$

$$\boldsymbol{\psi}_j(\mathbf{x}) := 4\sum_{i=1}^{d+1}\lambda_i\frac{\partial\lambda_i}{\partial x_j}(V_{\Gamma_i}-\mathbf{x}) \qquad \text{for } j=1\dots d.$$

Enumerate the basis functions from Definition 6.2 as $\boldsymbol{\psi}_l$, $l=1\dots 8$, for $d=2$ and $l=1\dots 15$ for $d=3$. For any $\mathbf{t}_h^i \in \mathbf{RTN_1}(\mathcal{T}_h)$, we can write $\mathbf{t}_h^i|_K = \sum_l (\mathbf{t}_h^i)_l\boldsymbol{\psi}_l$ with $(\mathbf{t}_h^i)_l$ the associated degrees of freedom. Recall that $\mathbf{t}_h^i = \mathbf{d}_h^i + \mathbf{a}_h^i$. Let $K\in\mathcal{T}_h$ be fixed. Then the coefficients $(\mathbf{d}_h^i)_l$ are given by (3.4a) and (3.4b). The coefficients of $\mathbf{a}_h^i$ are defined analogously following Definition 3.3.

The evaluation of a posteriori error estimators in Corollary 3.8 can be done again without factual construction of reconstructions as in Section 6.1. In particular, one needs a quadrature rule that is exact for quartic polynomials. Let

$$V_{ij}^{(3,1,0)} := \frac{3}{4}V_{\Gamma_i}+\frac{1}{4}V_{\Gamma_j} \qquad 1\le i,j\le d+1, i\ne j,$$

$$V_{ij}^{(2,2,0)} := \frac{1}{2}V_{\Gamma_i}+\frac{1}{2}V_{\Gamma_j} \qquad 1\le i<j\le d+1,$$

$$V_{ijk}^{(2,1,1)} := \frac{1}{2}V_{\Gamma_i}+\frac{1}{4}V_{\Gamma_j}+\frac{1}{4}V_{\Gamma_k} \qquad 1\le i,j,k\le d+1, i\ne j<k.$$

Then such a formula is, see [27],

$$\int_K w(\mathbf{x})\,\mathrm{d}\mathbf{x} \approx \begin{cases} \frac{4|K|}{45}\sum\limits_{1\le i,j\le 3, i\ne j} w(V_{ij}^{(3,1,0)}) - \frac{|K|}{45}\sum\limits_{1\le i<j\le 3} w(V_{ij}^{(2,2,0)}) \\ \quad +\frac{8|K|}{45}\sum\limits_{1\le i,j,k\le 3, i\ne j<k} w(V_{ijk}^{(2,1,1)}), & \text{for } d=2,\\ \frac{-5|K|}{420}\sum\limits_{k=1}^{4} w(V_{\Gamma_k}) + \frac{16|K|}{420}\sum\limits_{1\le i,j\le 4, i\ne j} w(V_{ij}^{(3,1,0)}) \\ \quad -\frac{12|K|}{420}\sum\limits_{1\le i<j\le 4} w(V_{ij}^{(2,2,0)}) + \frac{16|K|}{420}\sum\limits_{1\le i,j,k\le 4, i\ne j<k} + w(V_{ijk}^{(2,1,1)}) \\ \quad +\frac{128|K|}{420}w(\mathbf{x}_g), & \text{for } d=3,\end{cases}$$

where $\mathbf{x}_g$ is the barycentre of the simplex K.

7 Numerical experiments

In this section we will illustrate the behavior of the error estimates introduced in Section 3 and of the adaptive solution algorithm introduced in Section 4.

Algorithm 4.1 is applied with parameters $\nu^*=15$ and $\gamma_{\mathrm{rem}}=\gamma_{\mathrm{alg}}=10^{-1}$. We use the GMRES method [26] with ILU(0) preconditioning in order to solve the system (2.8). Our computations were carried out imposing three types of stopping criteria. Namely, *local stopping criteria* (4.1), *global stopping criteria* (4.2), and *classical stopping criteria*, where the last means that GMRES method was let to converge to a certain tolerance for the relative preconditioned algebraic residuum measured in the ℓ^2-norm. This tolerance has been chosen as big as possible such that the precision of the results is comparable with those when the local stopping criteria are applied. In the example below such a tolerance is 10^{-6}. Note that using a still smaller tolerance, as often done in practice, would favor even more our approach.

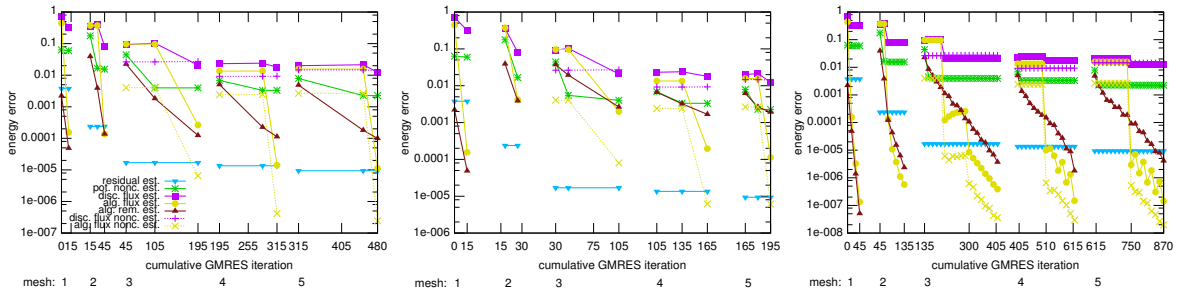

Figure 5: Development of the estimators on the individual meshes for local (left), global (middle), and classical stopping criteria (right)

7.1 Example with a smooth solution

We consider $\Omega \in (0,1) \times (0,1)$ and prescribe the source term in such a way that the exact solution has the following form:

$$u(x_1, x_2) = \sin(2\pi(x_1 + x_2)).$$

We employ the incomplete interior penalty DGM, i.e., (2.7) with $\theta = 0$, with the penalty parameter $\alpha_\gamma = 20$ for all $\gamma \in \mathcal{F}_h$ on triangular meshes possibly containing hanging nodes. The approximate solution is sought in the space $S_h^{\mathbf{2}}$, $\mathbf{2} := \{2_K\}_{K \in \mathcal{T}_h}$, and the flux reconstructions in the RTN space $\mathbf{RTN_2}(\mathcal{T}_h)$. The discretization flux reconstruction is defined by (3.4a) and (3.4b) whereas the algebraic error flux reconstruction by (3.5).

The computation is started with zero initial approximation for GMRES solver on a triangular conforming grid with 288 elements. Meshes are generated adaptively according to the elementwise discretization estimator (3.20a). Since we aim at fulfilling the condition $\eta^i_{\mathrm{disc}} \leq \omega$ for some tolerance ω, we require

$$\eta^i_{\mathrm{disc},K} \leq \frac{\omega}{\mathrm{card}(\mathcal{T}_h)^{\frac{1}{2}}} \tag{7.1}$$

to hold for all $K \in \mathcal{T}_h$, where $\mathrm{card}(\mathcal{T}_h)$ denotes the number of triangles in the current mesh. Therefore, triangles for those the condition (7.1) is violated are split into four smaller ones. The tolerance ω has been set to $3.3\,10^{-2}$ in the computations. In what follows, we display results for five successive meshes resulting from four levels of adaptation.

First, we show the behavior of individual estimators as defined in (3.12a), (3.12b), and (3.21). Results on the original mesh and first, second, third, and fourth adaptively refined meshes are displayed in Figure 5. Discretization and algebraic flux nonconformity estimators are not displayed for first two meshes as no hanging nodes are present and consequently they are zero (recall that we consider the same polynomial degree over the whole mesh). While the discretization flux estimator dominates on first two meshes, flux nonconformity estimators join on subsequent meshes where hanging nodes occur. We can see that the residual estimator is not substantial in comparison with other estimators as it is by one order of magnitude smaller on the first mesh and by two orders of magnitude smaller on subsequent meshes. Substantial estimators include flux estimators and potential nonconformity estimators. It is important to note that in all three cases, the values and behavior of the discretization estimators are very close.

Further, we are interested in how the estimators of the total, discretization, and algebraic error (see respectively the right-hand side of (3.13), (3.20a), and (3.20b)) correspond to the *actual errors*. In Figure 6 evolution of these estimators through the whole adaptation process as a function of mesh adaptation is displayed.

Subsequent series of figures compare actual and estimated distribution of the total, discretization, and algebraic errors when local stopping criteria (4.1) are applied. We can see that our prediction of *distribution* of the discretization error is sharp on meshes not including hanging nodes whereas such a sharpness is lost a bit when hanging nodes appear. That is the price we pay for an economical computation of flux reconstructions as we do not construct a matching submesh of the original (nonmatching) mesh. Gratifyingly, Figures 9, 12, 15, 18, and 21 show that our estimates provide sharp prediction of the algebraic error even on meshes with hanging nodes.

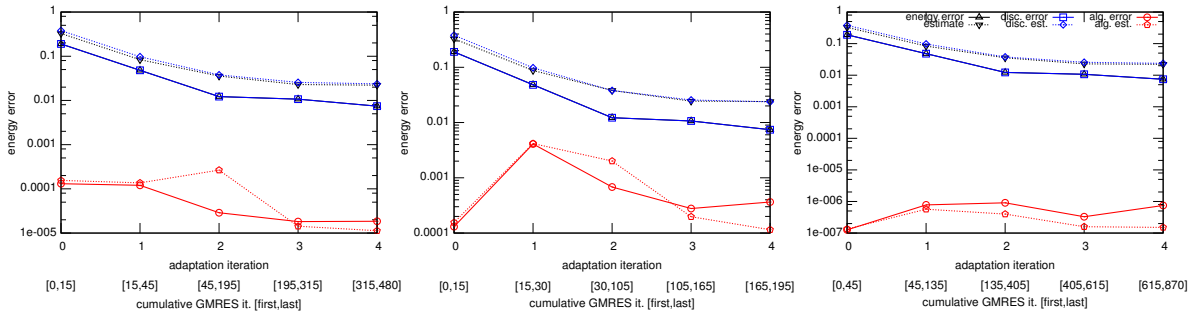

Figure 6: Development of the total, discretization, and algebraic error and the respective estimates during the adaptive process for local (left), global (middle), and classical stopping criteria (right)

Finally, Figure 22 (left) compares energy error of the computational solution u_h^i and Figure 22 (right) the effectivity index as a function of (accumulated) GMRES iterations for the individual stopping criteria. We observe that local stopping criteria lead to significant computational savings compared to classical stopping criteria, with a minimal loss of accuracy. In order to achieve a given value of the energy error, much more GMRES iterations are required for the classical stopping criteria in comparison with the local stopping criteria. Global stopping criteria enable still more economical calculation without precision loss in this first test case without singularity. Finally, we can see that the effectivity index jumps depending on the increase or decrease of the number of hanging nodes. More precisely, its value is close to 1.7 on meshes without hanging nodes and increases a little bit close to 3 when hanging nodes appear.

7.2 Example with a steep gradient solution

We consider $\Omega \in (0,1) \times (0,1)$ and prescribe the source term in such a way that the exact solution has the following form:

$$u(x_1, x_2) = \arctan(36x_1).$$

We employ the same initial computational setting as in the previous example. In particular, the approximate solution is sought in the space $S_h^{\mathbf{2}}$, $\mathbf{2} := \{2_K\}_{K \in \mathcal{T}_h}$, and the flux reconstructions in the RTN space $\mathbf{RTN_2}(\mathcal{T}_h)$. As in the previous example, we show results for five successive meshes resulting from four levels of adaptation. The behavior of individual estimators as defined in (3.12a), (3.12b), and (3.21) on all computational meshes is displayed in Figure 23. In this example, only the original mesh is without hanging nodes. Therefore, discretization and algebraic flux nonconformity estimators are zero just on that mesh. The number of hanging nodes is much smaller in comparison with the first example 7.1. As a result, the flux nonconformity estimators are not dominant in this example even on meshes with hanging nodes. As in the first example 7.1, we observe that the residual estimator is by one to two orders of magnitude smaller on the individual meshes and that the values and behavior of the discretization estimators for the individual stopping criteria are very close. In Figure 24 evolution of the estimators of the total, discretization, and algebraic error (see respectively the right-hand side of (3.13), (3.20a), and (3.20b)) through the whole adaptation process as a function of mesh adaptation is displayed.

Further, Figures 25-39 compare actual and estimated distribution of the total, discretization, and algebraic errors when local stopping criteria (4.1) are applied. We can see that the steep gradient region is well predicted (see Figures 26, 29, 32, 35, and 38), however, in fine meshes of Figures 35 and 38 the discretization error is overestimated in triangles with a hanging node. As in the first example 7.1, our estimates provide sharp prediction of the algebraic error.

Finally, Figure 40 (left) compares energy error of the computational solution u_h^i and Figure 40 (right) the effectivity index as a function of (accumulated) GMRES iterations for the individual stopping criteria. We observe that local stopping criteria lead to just slight computational savings (10% of GMRES iterations exactly) compared to classical stopping criteria, with a minimal loss of accuracy. On the contrary, global stopping criteria require about half of iterations less with subtle precision loss. Further, we can see that the variation of the effectivity index is not much influenced by the presence of hanging nodes as the number of hanging nodes is not substantial in comparison with the number of triangles.

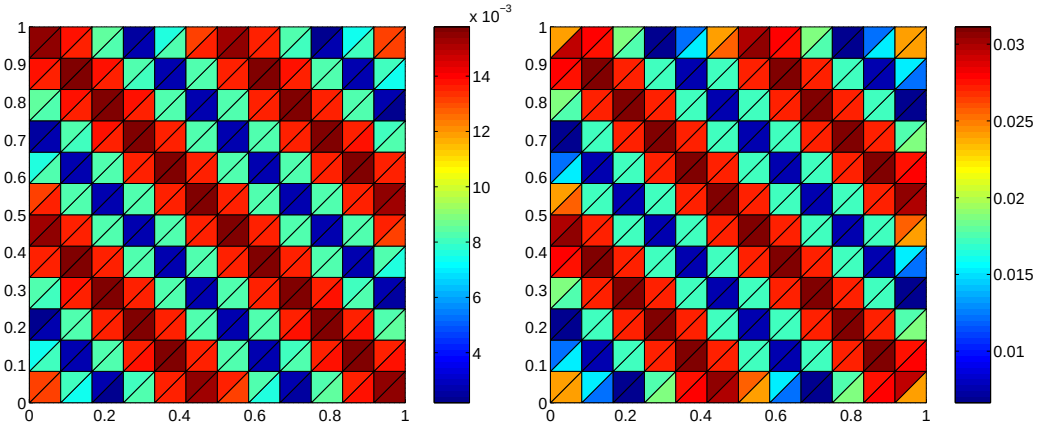

Figure 7: Distribution of the total error (left) and its estimate (right) on the first mesh

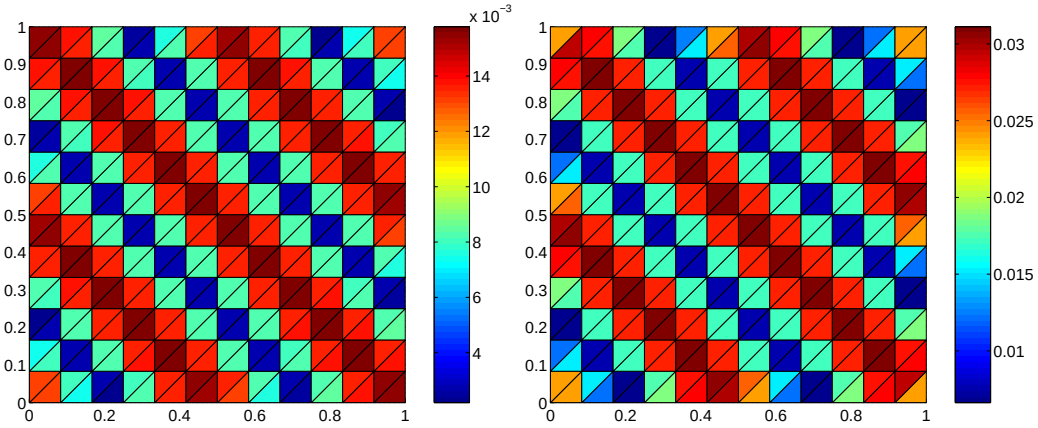

Figure 8: Distribution of the discretization error (left) and its estimate (right) on the first mesh

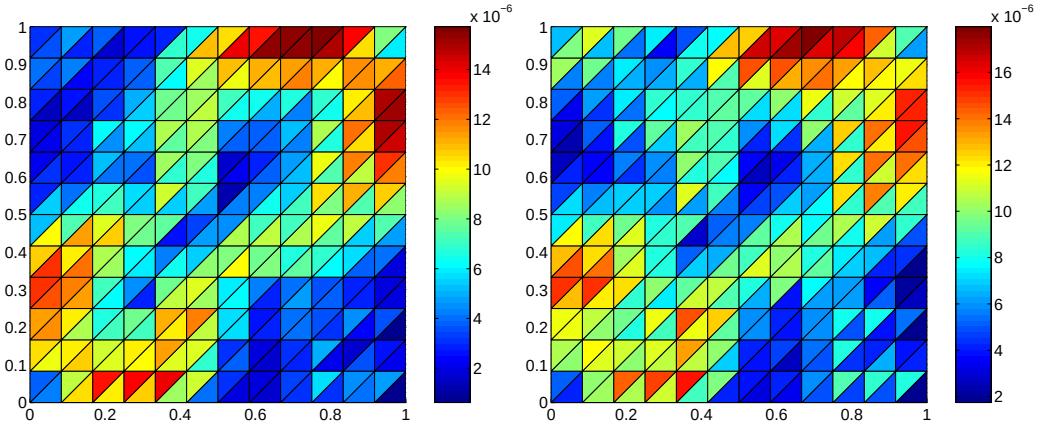

Figure 9: Distribution of the algebraic error (left) and its estimate (right) on the first mesh

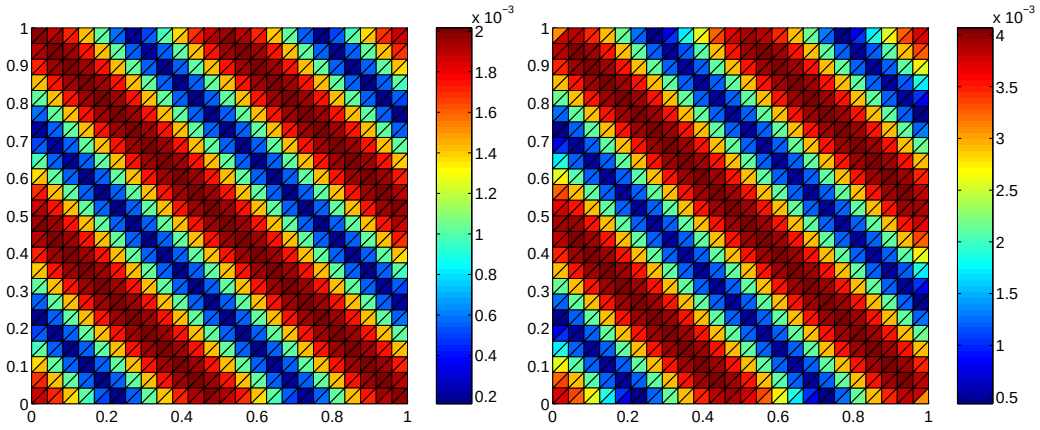

Figure 10: Distribution of the total error (left) and its estimate (right) on the second mesh

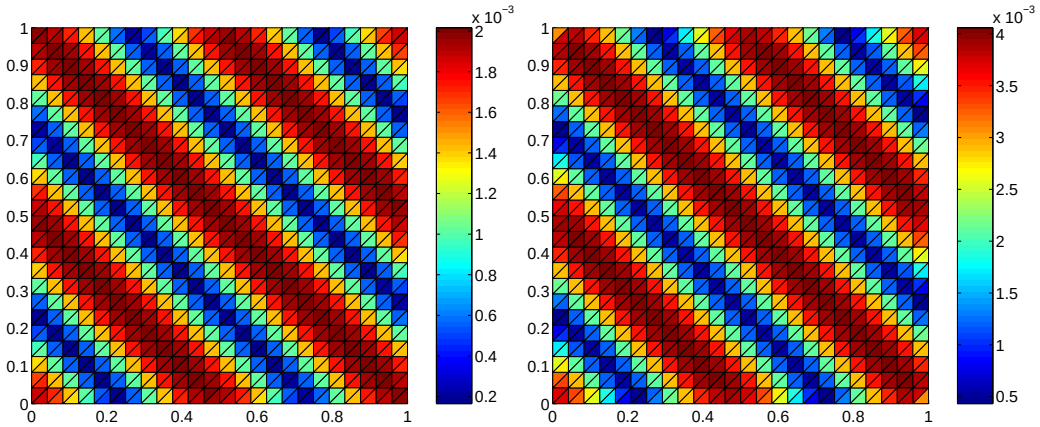

Figure 11: Distribution of the discretization error (left) and its estimate (right) on the second mesh

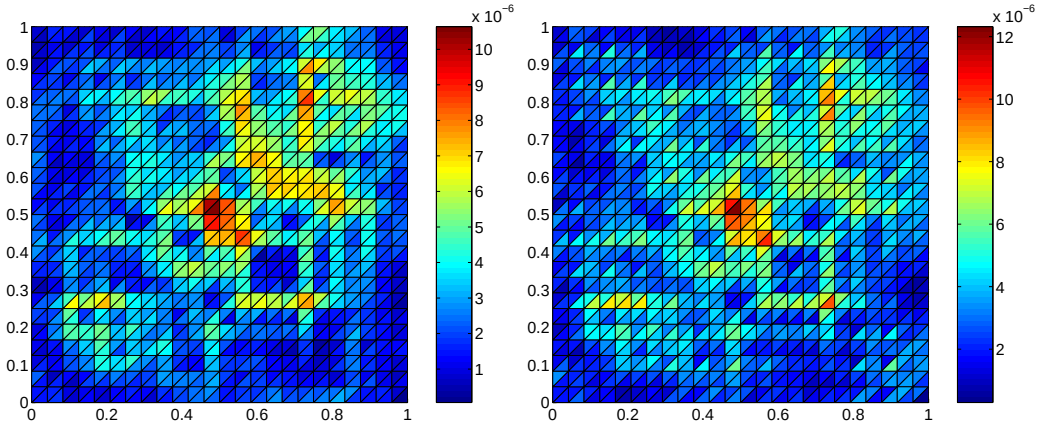

Figure 12: Distribution of the algebraic error (left) and its estimate (right) on the second mesh

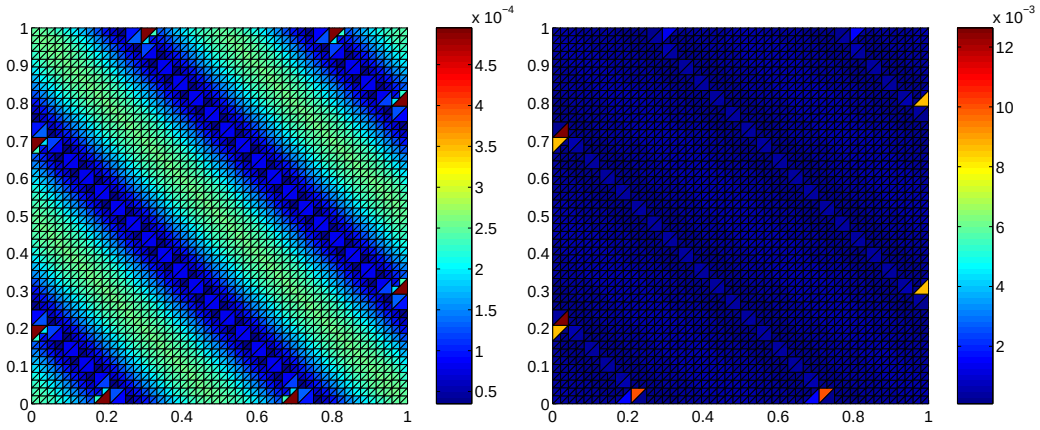

Figure 13: Distribution of the total error (left) and its estimate (right) on the third mesh

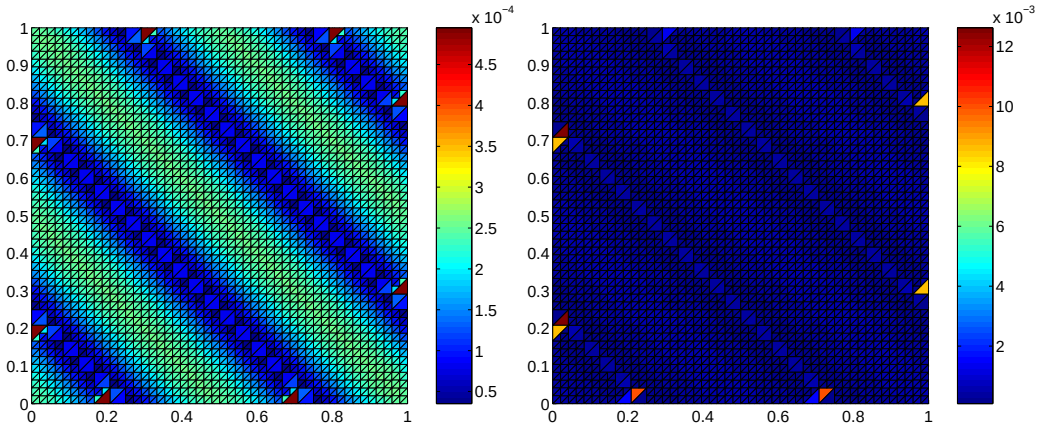

Figure 14: Distribution of the discretization error (left) and its estimate (right) on the third mesh

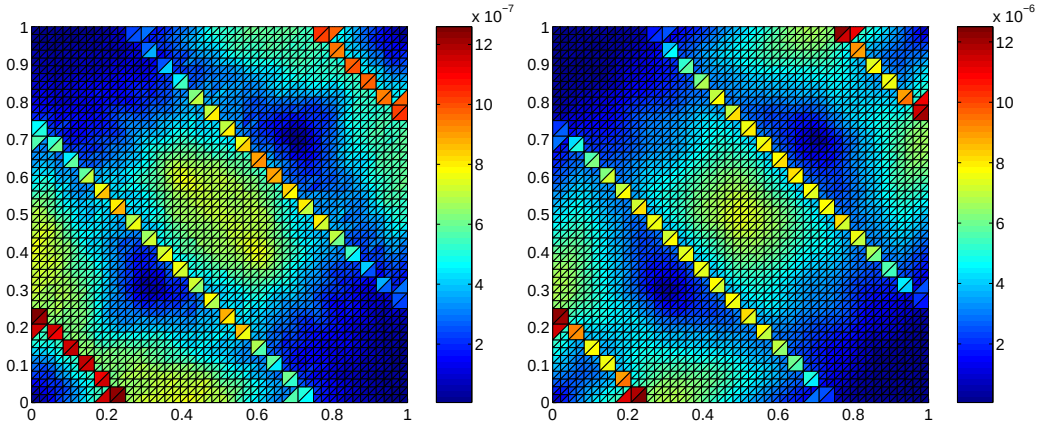

Figure 15: Distribution of the algebraic error (left) and its estimate (right) on the third mesh

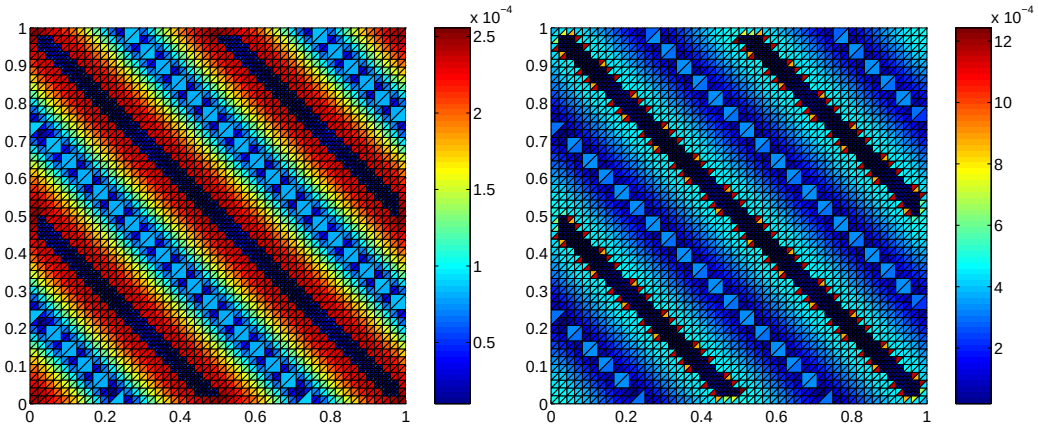

Figure 16: Distribution of the total error (left) and its estimate (right) on the fourth mesh

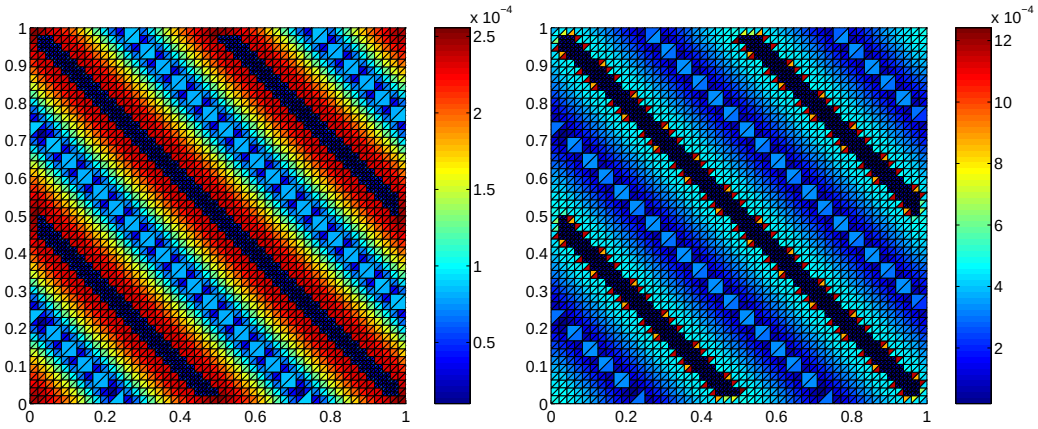

Figure 17: Distribution of the discretization error (left) and its estimate (right) on the fourth mesh

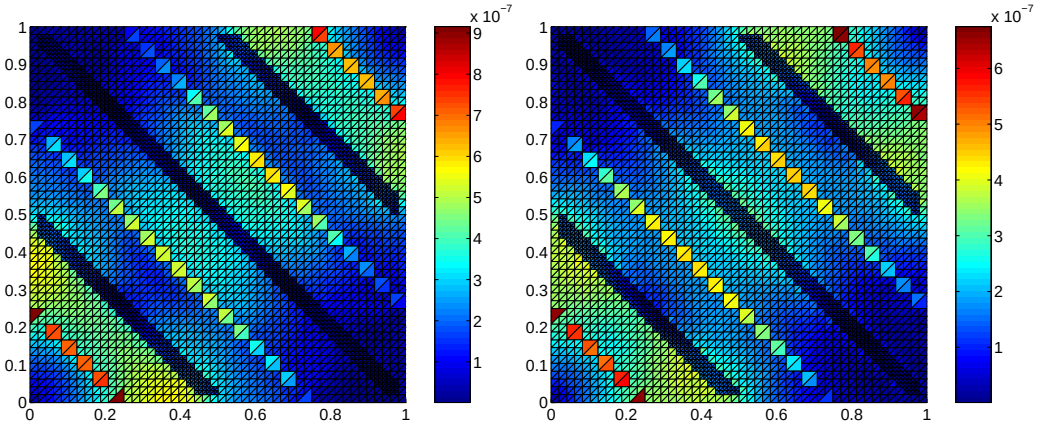

Figure 18: Distribution of the algebraic error (left) and its estimate (right) on the fourth mesh

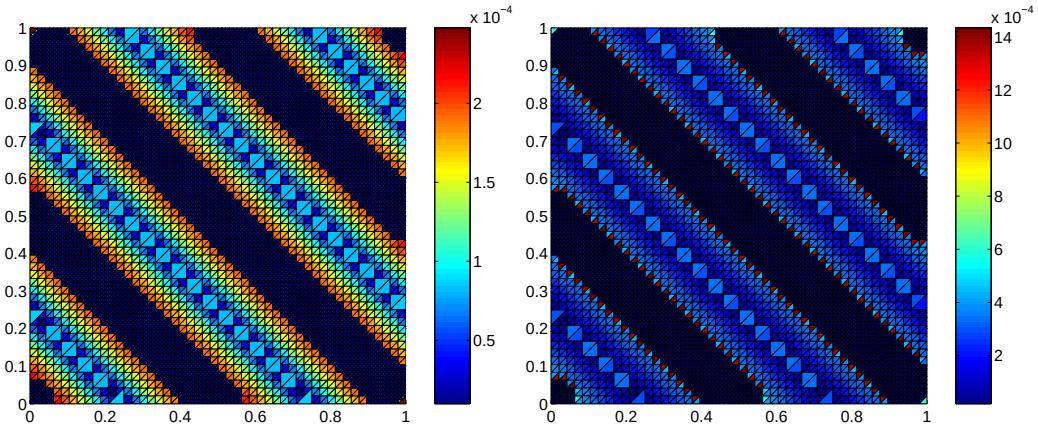

Figure 19: Distribution of the total error (left) and its estimate (right) on the fifth mesh

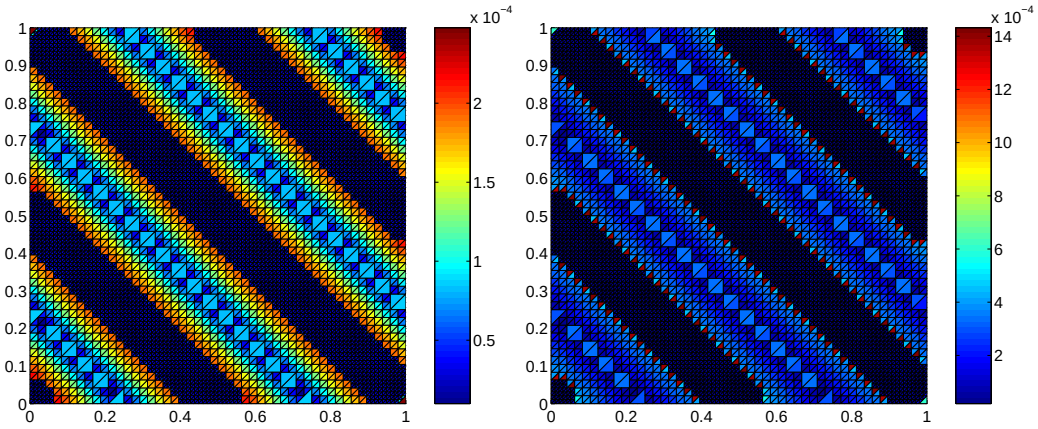

Figure 20: Distribution of the discretization error (left) and its estimate (right) on the fifth mesh

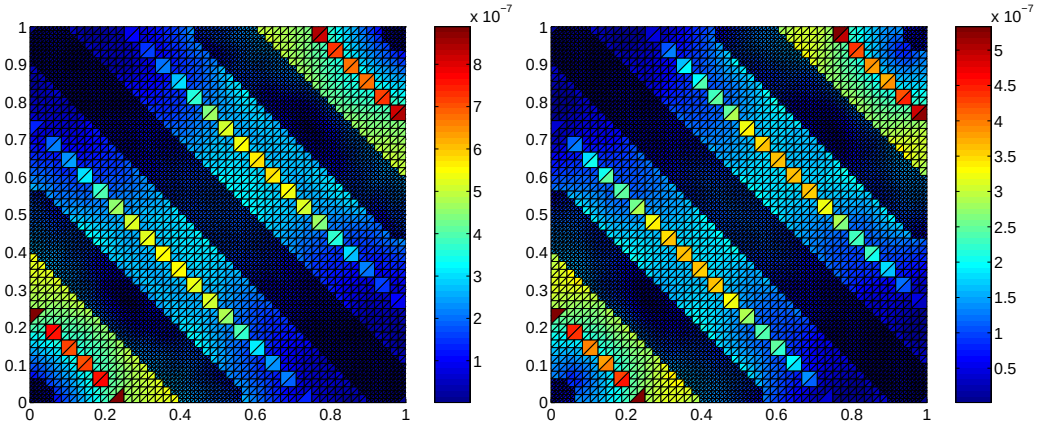

Figure 21: Distribution of the algebraic error (left) and its estimate (right) on the fifth mesh

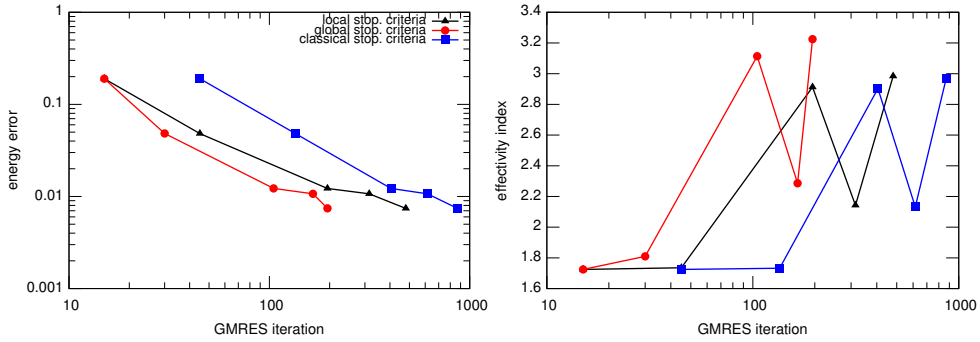

Figure 22: Comparison of energy error (left) and of effectivity indices (right) for individual stopping criteria

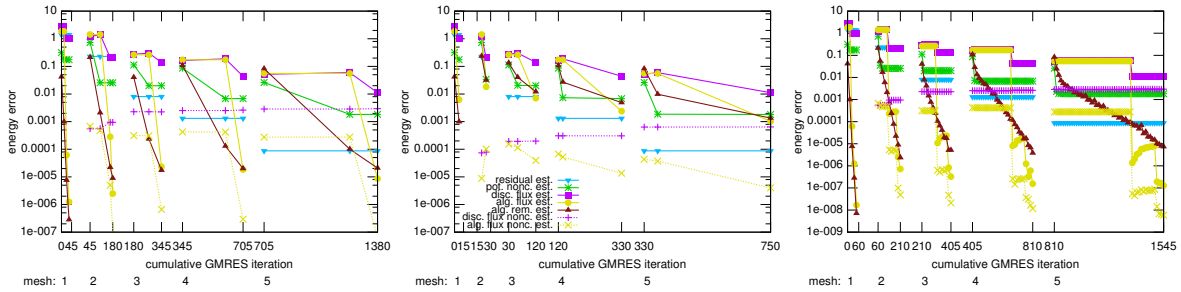

Figure 23: Development of the estimators on the individual meshes for local (left), global (middle), and classical stopping criteria (right)

References

[1] M. Ainsworth, *A posteriori error estimation for discontinuous Galerkin finite element approximation*, SIAM J. Numer. Anal., 45 (2007), pp. 1777–1798.

[2] M. Ainsworth and R. Rankin, *Fully computable error bounds for discontinuous Galerkin finite element approximations on meshes with an arbitrary number of levels of hanging nodes*, SIAM J. Numer. Anal., 47 (2010), pp. 4112–4141.

[3] ———, *Constant free error bounds for nonuniform order discontinuous Galerkin finite-element approximation on locally refined meshes with hanging nodes*, IMA J. Numer. Anal., 31 (2011), pp. 254–280.

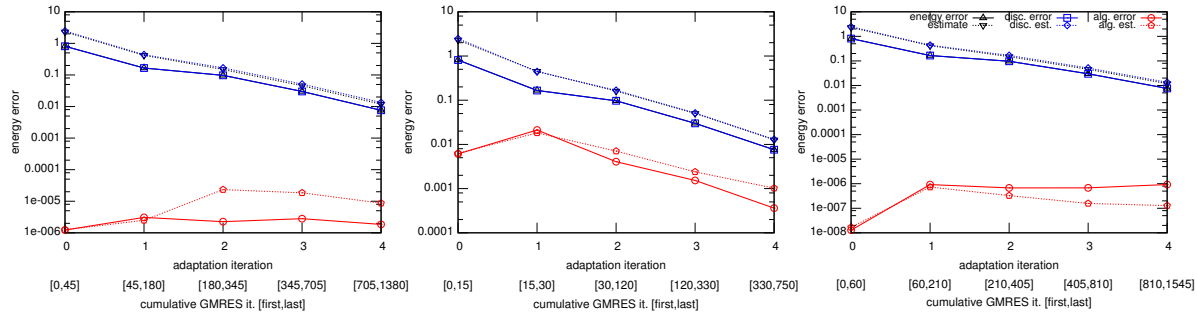

Figure 24: Development of the total, discretization, and algebraic error and the respective estimates during the adaptive process for local (left), global (middle), and classical stopping criteria (right)

[4] M. Arioli, *A stopping criterion for the conjugate gradient algorithm in a finite element method framework*, Numer. Math., 97 (2004), pp. 1–24.

[5] M. Arioli, J. Liesen, A. Międlar, and Z. Strakoš, *Interplay between discretization and algebraic computation in adaptive numerical solution of elliptic PDE problems.* GAMM Mitteilungen, to appear, 2013.

[6] M. Arioli, D. Loghin, and A. J. Wathen, *Stopping criteria for iterations in finite element methods*, Numer. Math., 99 (2005), pp. 381–410.

[7] R. Becker, C. Johnson, and R. Rannacher, *Adaptive error control for multigrid finite element methods*, Computing, 55 (1995), pp. 271–288.

[8] F. Brezzi and M. Fortin, *Mixed and hybrid finite element methods*, vol. 15 of Springer Series in Computational Mathematics, Springer-Verlag, New York, 1991.

[9] S. Cochez-Dhondt and S. Nicaise, *Equilibrated error estimators for discontinuous Galerkin methods*, Numer. Methods Partial Differential Equations, 24 (2008), pp. 1236–1252.

[10] D. A. Di Pietro and A. Ern, *Mathematical aspects of discontinuous Galerkin methods*, vol. 69 of Mathématiques & Applications (Berlin) [Mathematics & Applications], Springer, Heidelberg, 2012.

[11] A. Ern, S. Nicaise, and M. Vohralík, *An accurate* $\mathbf{H}(\mathrm{div})$ *flux reconstruction for discontinuous Galerkin approximations of elliptic problems*, C. R. Math. Acad. Sci. Paris, 345 (2007), pp. 709–712.

[12] A. Ern, A. F. Stephansen, and M. Vohralík, *Guaranteed and robust discontinuous Galerkin a posteriori error estimates for convection–diffusion–reaction problems*, J. Comput. Appl. Math., 234 (2010), pp. 114–130.

[13] A. Ern and M. Vohralík, *Flux reconstruction and a posteriori error estimation for discontinuous Galerkin methods on general nonmatching grids*, C. R. Math. Acad. Sci. Paris, 347 (2009), pp. 441–444.

[14] ———, *Adaptive inexact Newton methods with a posteriori stopping criteria for nonlinear diffusion PDEs*, SIAM J. Sci. Comput., 35 (2013), pp. A1761–A1791.

[15] P. Jiránek, Z. Strakoš, and M. Vohralík, *A posteriori error estimates including algebraic error and stopping criteria for iterative solvers*, SIAM J. Sci. Comput., 32 (2010), pp. 1567–1590.

[16] O. A. Karakashian and F. Pascal, *A posteriori error estimates for a discontinuous Galerkin approximation of second-order elliptic problems*, SIAM J. Numer. Anal., 41 (2003), pp. 2374–2399.

[17] K. Y. Kim, *A posteriori error analysis for locally conservative mixed methods*, Math. Comp., 76 (2007), pp. 43–66.

[18] ———, *A posteriori error estimators for locally conservative methods of nonlinear elliptic problems*, Appl. Numer. Math., 57 (2007), pp. 1065–1080.

[19] J. Liesen and Z. Strakoš, *Krylov Subspace Methods. Principles and Analysis*, Numerical Mathematics and Scientific Computation, Oxford University Press, Oxford, United Kingdom, 2013.

[20] D. Meidner, R. Rannacher, and J. Vihharev, *Goal-oriented error control of the iterative solution of finite element equations*, J. Numer. Math., 17 (2009), pp. 143–172.

[21] S. Nicaise, *A posteriori error estimations of some cell-centered finite volume methods*, SIAM J. Numer. Anal., 43 (2005), pp. 1481–1503.

[22] G. V. Pencheva, M. Vohralík, M. F. Wheeler, and T. Wildey, *Robust a posteriori error control and adaptivity for multiscale, multinumerics, and mortar coupling*, SIAM J. Numer. Anal., 51 (2013), pp. 526–554.

[23] A. Quarteroni and A. Valli, *Numerical approximation of partial differential equations*, vol. 23 of Springer Series in Computational Mathematics, Springer-Verlag, Berlin, 1994.

[24] R. Rannacher, A. Westenberger, and W. Wollner, *Adaptive finite element solution of eigenvalue problems: balancing of discretization and iteration error*, J. Numer. Math., 18 (2010), pp. 303–327.

[25] K. Rektorys, *Variational methods in mathematics, science and engineering*, D. Reidel Publishing Co., Dordrecht, 1977. Translated from the Czech by Michael Basch.

[26] Y. Saad and M. H. Schultz, *GMRES: a generalized minimal residual algorithm for solving non-symmetric linear systems*, SIAM J. Sci. Statist. Comput., 7 (1986), pp. 856–869.

[27] P. Silvester, *Symmetric quadrature formulae for simplexes*, Math. Comp., 24 (1970), pp. 95–100.

[28] R. Verfürth, *A review of a posteriori error estimation and adaptive mesh-refinement techniques*, Teubner-Wiley, Stuttgart, 1996.

[29] M. F. Wheeler and I. Yotov, *A posteriori error estimates for the mortar mixed finite element method*, SIAM J. Numer. Anal., 43 (2005), pp. 1021–1042.

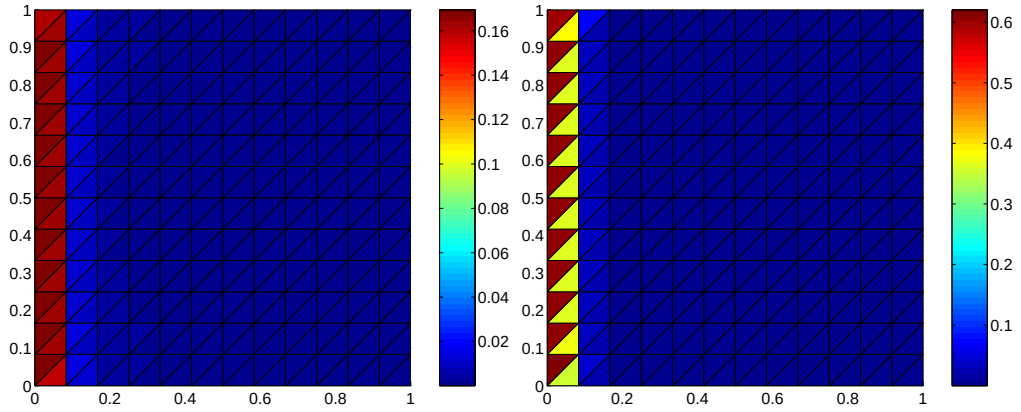

Figure 25: Distribution of the total error (left) and its estimate (right) on the first mesh

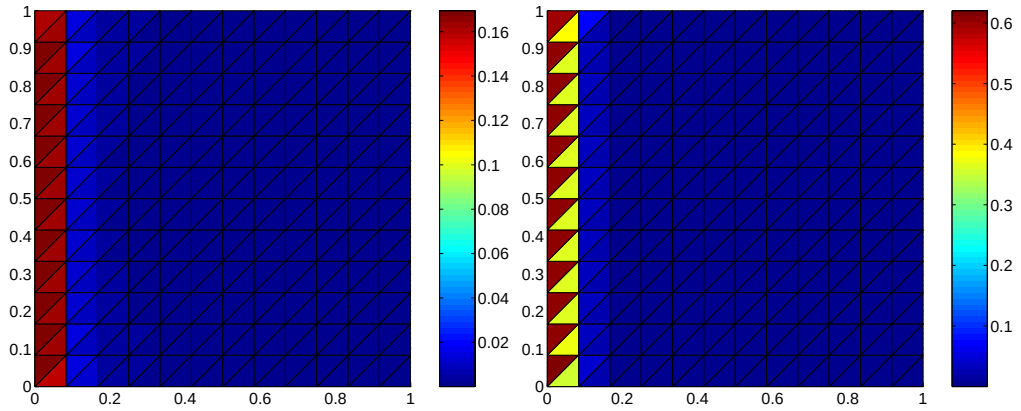

Figure 26: Distribution of the discretization error (left) and its estimate (right) on the first mesh

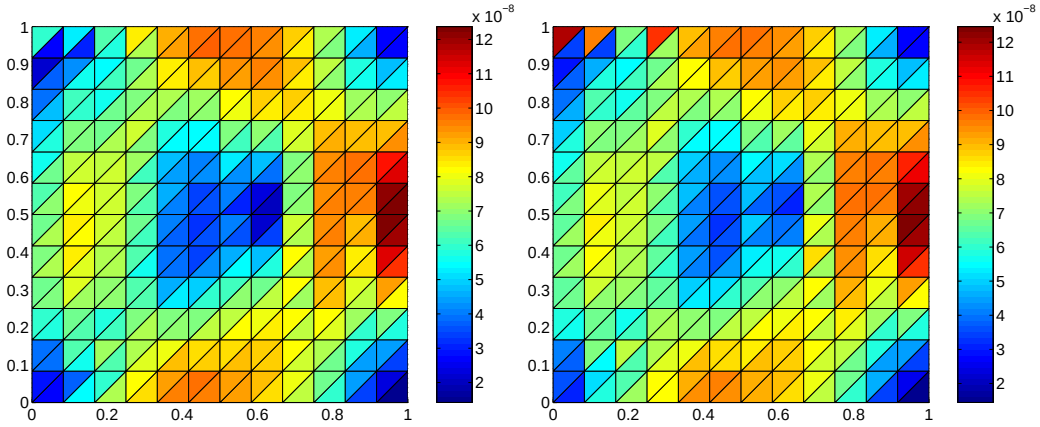

Figure 27: Distribution of the algebraic error (left) and its estimate (right) on the first mesh

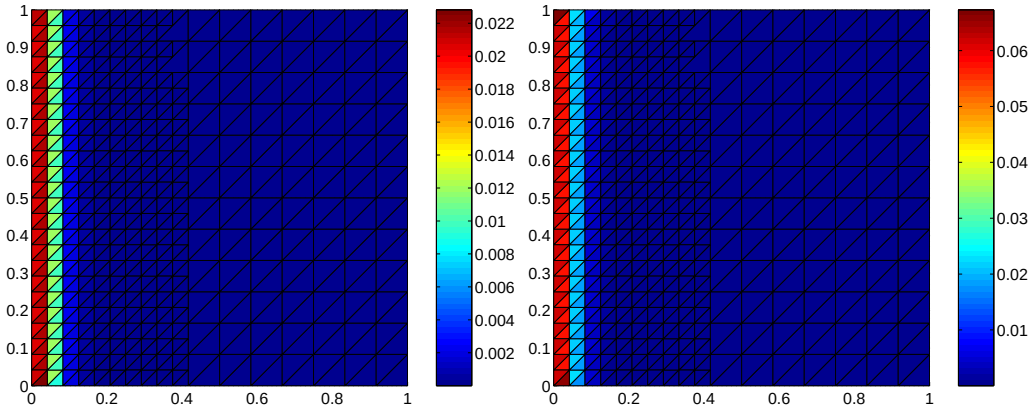

Figure 28: Distribution of the total error (left) and its estimate (right) on the second mesh

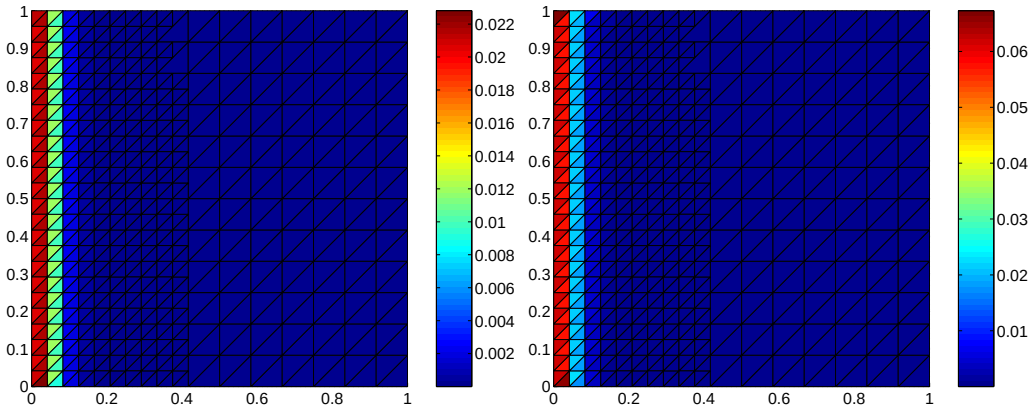

Figure 29: Distribution of the discretization error (left) and its estimate (right) on the second mesh

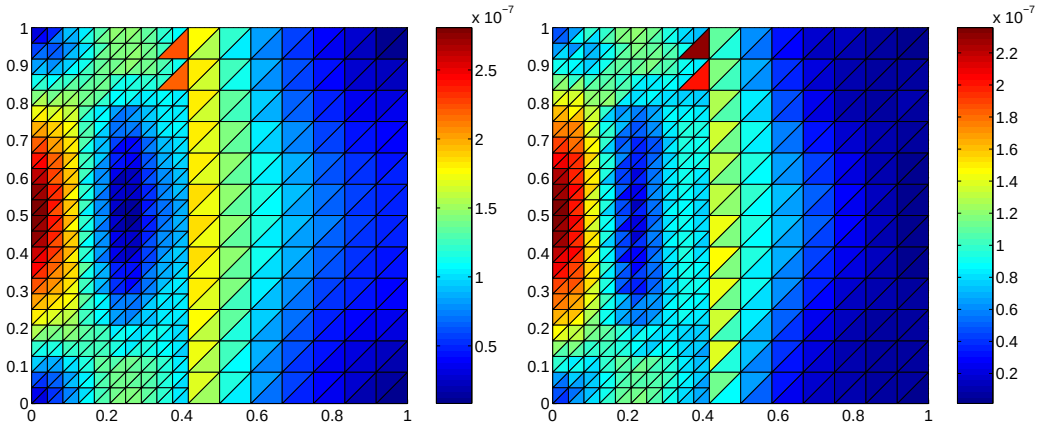

Figure 30: Distribution of the algebraic error (left) and its estimate (right) on the second mesh

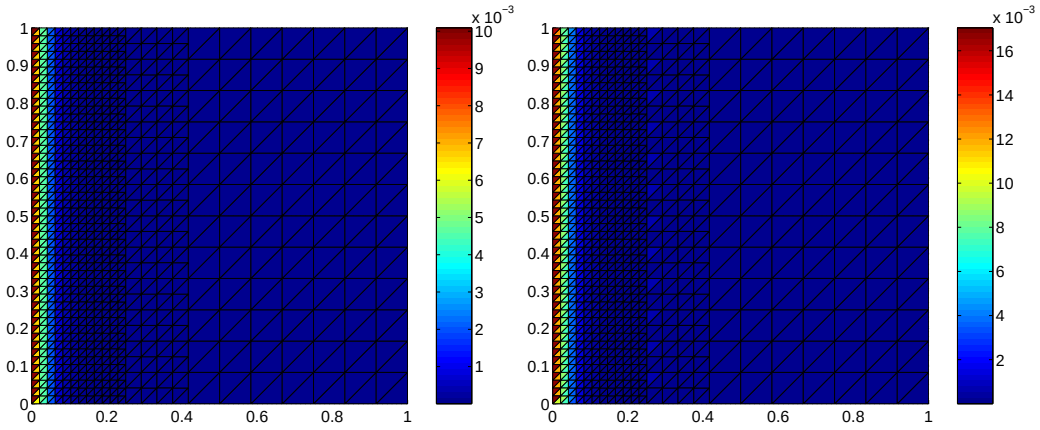

Figure 31: Distribution of the total error (left) and its estimate (right) on the third mesh

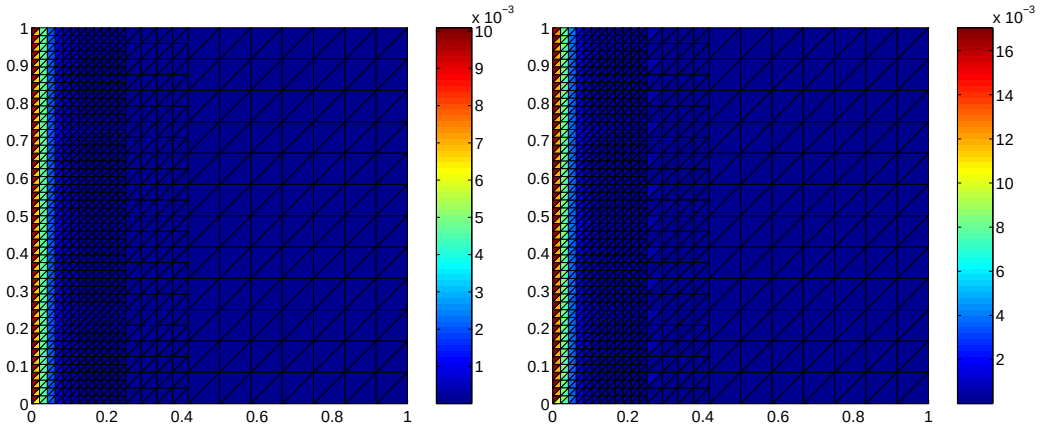

Figure 32: Distribution of the discretization error (left) and its estimate (right) on the third mesh

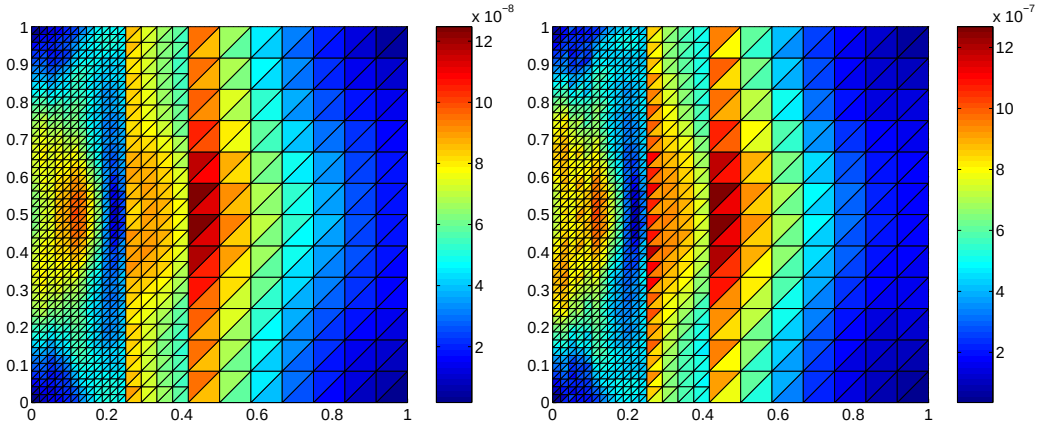

Figure 33: Distribution of the algebraic error (left) and its estimate (right) on the third mesh

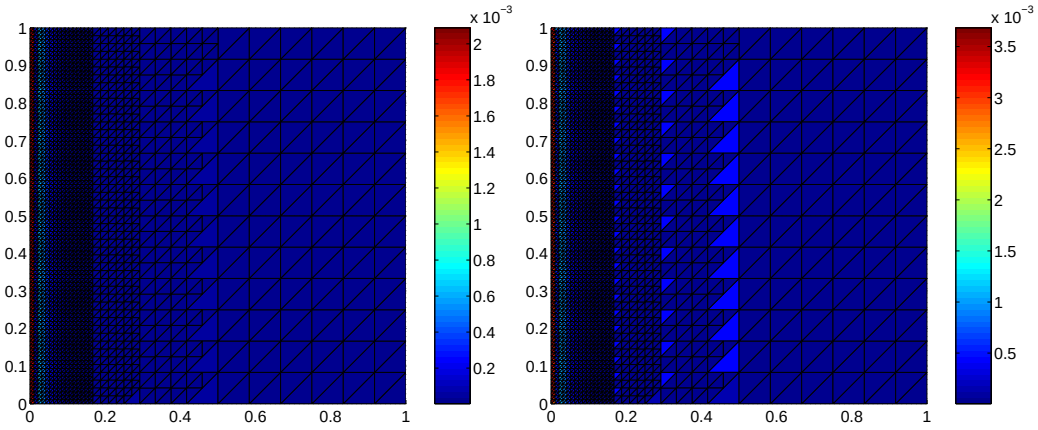

Figure 34: Distribution of the total error (left) and its estimate (right) on the fourth mesh

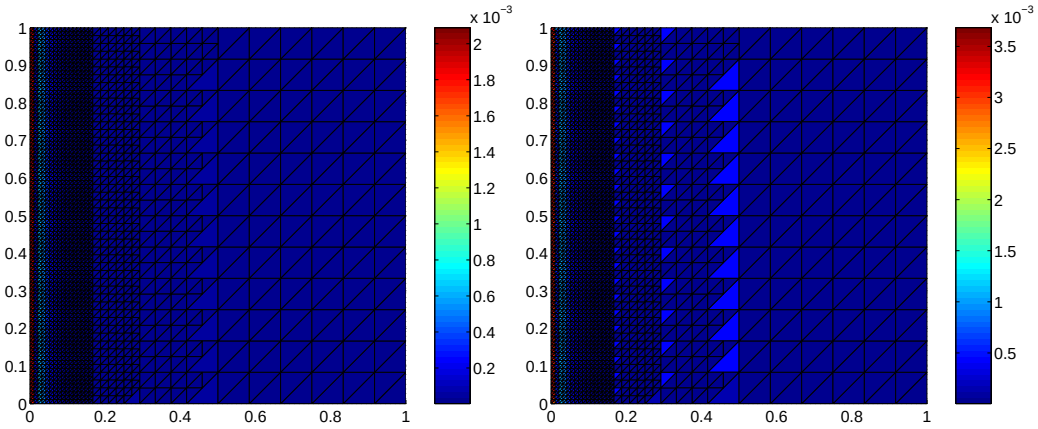

Figure 35: Distribution of the discretization error (left) and its estimate (right) on the fourth mesh

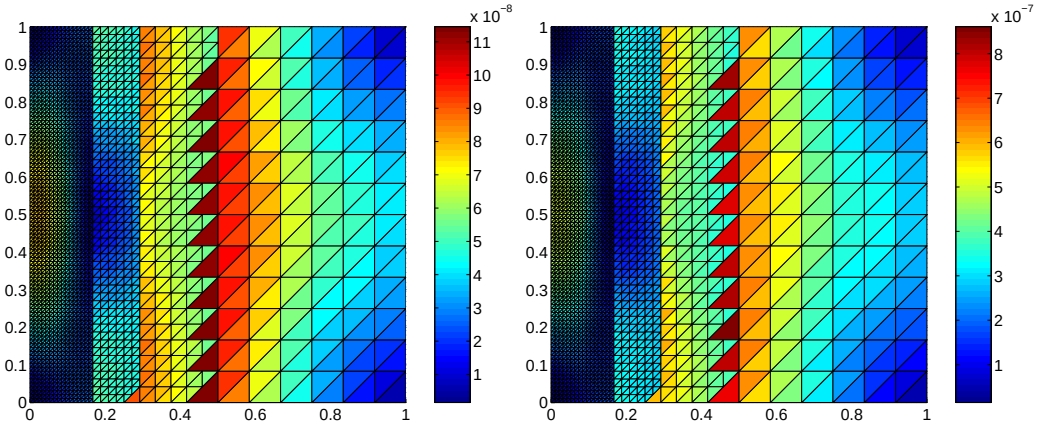

Figure 36: Distribution of the algebraic error (left) and its estimate (right) on the fourth mesh

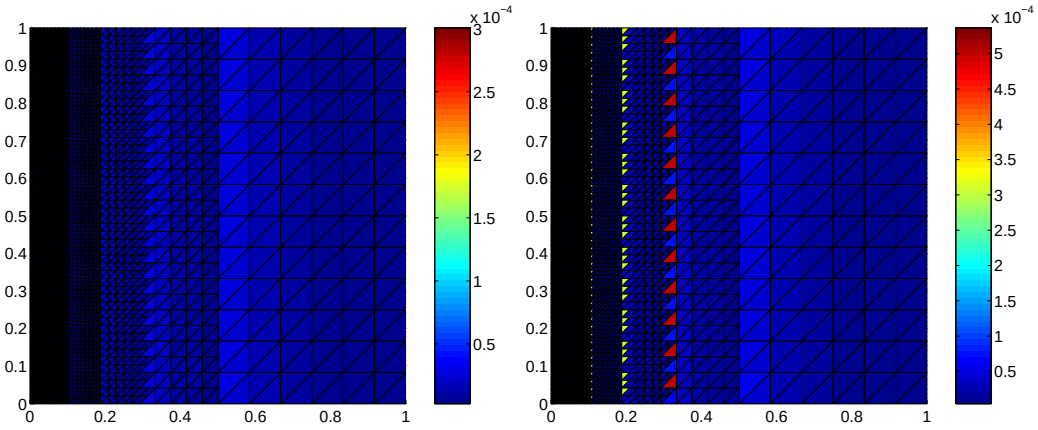

Figure 37: Distribution of the total error (left) and its estimate (right) on the fifth mesh

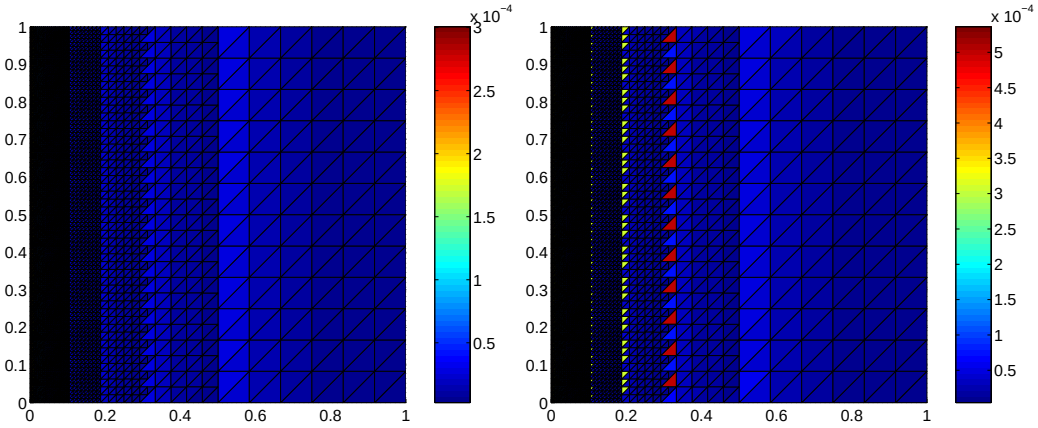

Figure 38: Distribution of the discretization error (left) and its estimate (right) on the fifth mesh

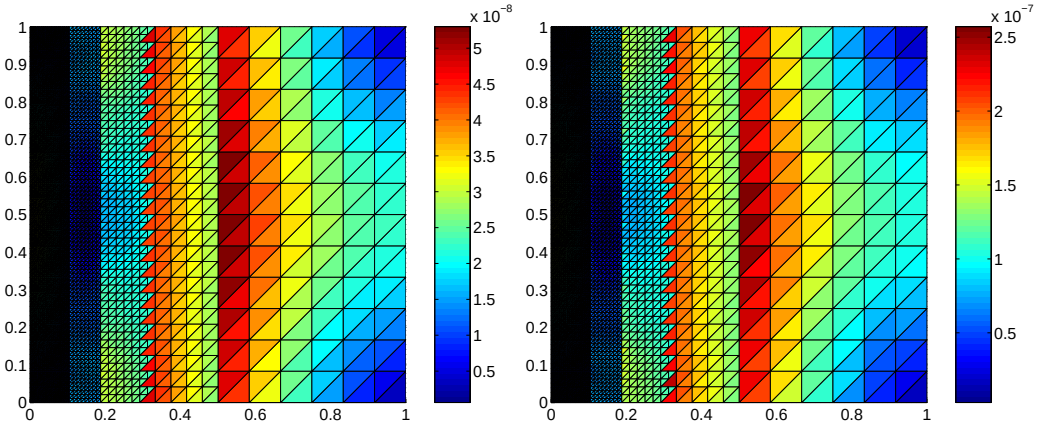

Figure 39: Distribution of the algebraic error (left) and its estimate (right) on the fifth mesh

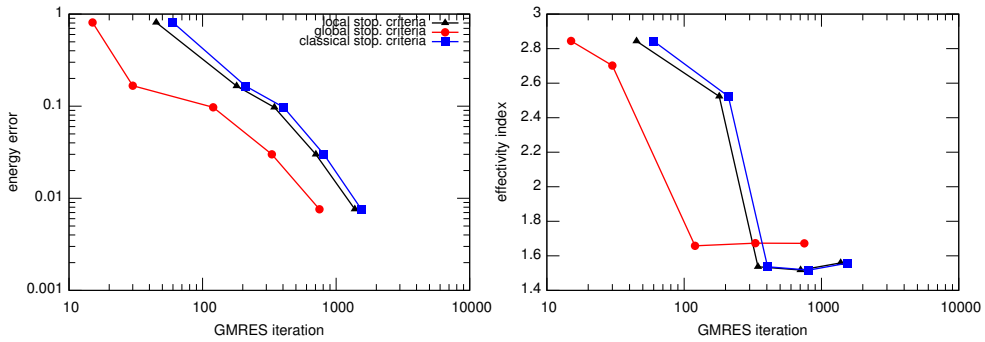

Figure 40: Comparison of energy error (left) and effectivity indices (right) for individual stopping criteria